

The Drivers of the Decline in Supermassive Black Hole Growth at $z < 2$

ZHIBO YU (喻知博) ^{1,2} W. N. BRANDT ^{1,2,3} FAN ZOU ⁴ BIN LUO ^{5,6} QINGLING NI ⁷ D. P. SCHNEIDER ^{1,2}
AND FABIO VITO ⁸

¹*Department of Astronomy and Astrophysics, The Pennsylvania State University, 525 Davey Lab, University Park, PA 16802, USA*

²*Institute for Gravitation and the Cosmos, The Pennsylvania State University, University Park, PA 16802, USA*

³*Department of Physics, The Pennsylvania State University, 104 Davey Laboratory, University Park, PA 16802, USA*

⁴*Department of Astronomy, University of Michigan, 1085 S University, Ann Arbor, MI 48109, USA*

⁵*School of Astronomy and Space Science, Nanjing University, Nanjing 210093, People's Republic of China*

⁶*Key Laboratory of Modern Astronomy and Astrophysics (Nanjing University), Ministry of Education, Nanjing 210093, People's Republic of China*

⁷*Max-Planck-Institut für extraterrestrische Physik (MPE), Gießenbachstraße 1, D-85748 Garching bei München, Germany*

⁸*INAF-Osservatorio di Astrofisica e Scienza dello Spazio di Bologna, Via Gobetti 93/3, I-40129 Bologna, Italy*

ABSTRACT

It is well established that cosmic supermassive black hole (SMBH) growth peaks at $z \approx 1.5 - 2$, followed by a strong decline of $\approx 1 - 1.5$ dex toward the present day, with the comoving number density of higher-luminosity active galactic nuclei (AGNs) peaking at higher redshift (referred to as “AGN downsizing”). We leverage the best current measurements of the SMBH accretion distribution, based upon data from nine well-characterized extragalactic fields with a “wedding-cake” design, to investigate and quantify the drivers of the drastic decline in cosmic SMBH growth. The decline in the typical Eddington ratio (λ_{Edd}) of AGNs (decreasing by ≈ 1.35 dex from $z \approx 1.5 - 2$ to $z \approx 0.2$) is the dominant driver for the broad decline in SMBH growth, rather than a shift of accretion activity to less-massive SMBHs. As λ_{Edd} decreases toward lower redshift, the primary contributor to the cosmic SMBH accretion density (ρ_{BHAR}) has shifted from high- λ_{Edd} AGNs to low- λ_{Edd} AGNs, even though the latter always dominate the comoving AGN number density at $z < 4$. We also find that the decline in SMBH growth toward lower SMBH mass in less-massive galaxies is primarily due to the decreasing outburst luminosity rather than the duty cycle.

Keywords: Supermassive black holes (1663) — X-ray active galactic nuclei (2035) — Galaxies (573)

1. INTRODUCTION

Understanding the growth history of supermassive black holes (SMBHs) is one of the most important topics for extragalactic studies. Observations have revealed tight correlations between black-hole mass (M_{BH}) and the host-galaxy bulge stellar mass/bulge velocity dispersion (e.g., J. Kormendy & L. C. Ho 2013). Furthermore, it has been found that the long-term averaged black-hole accretion rate ($\overline{\text{BHAR}}$), which is approximated by the sample-averaged BHAR, is correlated with host-galaxy properties such as total stellar mass (M_*) and bulge star-formation rate (SFR) over most of cosmic time (e.g., Y. Q. Xue et al. 2010; J. Aird et al. 2012, 2018; G. Yang et al. 2018, 2019; I. Delvecchio et al. 2020; F. Zou

et al. 2024). These relations indicate that SMBHs and host galaxies evolve in a coordinated manner. Therefore, tracing the growth history of SMBHs can provide insights into the mechanism that drives galaxy-SMBH coevolution.

SMBHs in the local universe are generally much more “quiescent” than their high-redshift counterparts. Observations show that the comoving SMBH accretion-rate density (ρ_{BHAR}) traced by the active galactic nucleus (AGN) luminosity function and the comoving number density of AGNs both increase from $z \approx 4$ to $z \approx 2$ (although the behavior at higher redshift is still not clear, e.g., C. L. Barlow-Hall & J. Aird 2025), peak at $z \approx 1.5 - 2$, and then drop significantly by $\approx 1 - 1.5$ dex by the present day (e.g., Y. Ueda et al. 2014; J. Aird et al. 2015; T. Miyaji et al. 2015; T. T. Ananna et al. 2019; G. Yang et al. 2018, 2023). Notably, the decline in

SMBH growth is also luminosity dependent: the number density of high-luminosity AGNs peaks at a higher redshift ($z \approx 2$) than that of lower-luminosity AGNs, which reaches a maximum at $z \approx 1$ (e.g., L. L. Cowie et al. 2003; Y. Ueda et al. 2003; A. J. Barger et al. 2005; G. Hasinger et al. 2005; Y. Ueda et al. 2014; W. N. Brandt & D. M. Alexander 2015; A. Peca et al. 2023; D. M. Alexander et al. 2025). This phenomenon is referred to as “AGN downsizing”. If AGN luminosity is strictly correlated with M_{BH} (i.e., with fixed Eddington ratio, λ_{Edd}), this result would appear to imply that massive SMBHs largely formed before most less-massive SMBHs, in contrast to the hierarchical formation of dark matter halos based upon the standard cold dark matter model.

This apparent contradiction can be reconciled if we regard AGN downsizing as the dying down of cosmic accretion rather than as a symptom of antihierarchical formation of SMBHs. One proposed explanation is that AGN downsizing may be due to the shift of accretion activity to lower- M_{BH} SMBHs with lower luminosity (e.g., T. M. Heckman et al. 2004). On the other hand, since it has been shown that λ_{Edd} for type 1 quasars has a broad distribution at $z < 5$ (e.g., A. Babić et al. 2007; Y. Shen & B. C. Kelly 2012; B. C. Kelly & Y. Shen 2013; A. Schulze et al. 2015; H. Suh et al. 2015), AGN downsizing may also be driven by a decrease in λ_{Edd} with low- λ_{Edd} AGNs having a greater contribution to ρ_{BHAR} and n_{AGN} at lower redshift. Indeed, since the coevolution between SMBHs and galaxies has been established, we should expect the typical SMBH accretion rate to decrease with cosmic time, similar to the observed decline in SFR (e.g., P. Madau & M. Dickinson 2014; K. E. Whitaker et al. 2014). Such coevolution is related to the decreasing gas supply and merger rate toward lower redshift, because galaxy-scale gas inflows and major mergers are known to drive both star-formation and SMBH fueling (e.g., T. Di Matteo et al. 2005; P. F. Hopkins & L. Hernquist 2006; P. F. Hopkins & E. Quataert 2010). It has been suggested that AGN downsizing is partly attributed to the decreasing merger rate toward lower redshift, because merger-induced accretion is thought to produce the most luminous accretion events, causing the earlier peak of ρ_{BHAR} and n_{AGN} for high-luminosity AGNs when major mergers are more frequent (e.g., E. Treister et al. 2012).

The broad decline in SMBH growth at $z \lesssim 1.5 - 2$ is also M_{\star} -dependent. It has been shown that $\overline{\text{BHAR}}$, which describes the average accretion rate *per galaxy*, decreases as M_{\star} decreases at fixed redshift (e.g., Y. Q. Xue et al. 2010; J. Aird et al. 2012, 2018; G. Yang et al. 2018; F. Zou et al. 2024). This appears to contrast with

the evolution of galaxy SFR at $z \lesssim 2$ where star formation preferentially stops in high-mass galaxies (e.g., K. E. Whitaker et al. 2014), if SMBHs strictly coevolve with their host galaxies. This indicates that SMBH growth is also influenced by physical processes distinct from those driving galaxy-wide star formation. For example, it is likely that more massive galaxies tend to host more massive and luminous SMBHs, and/or the AGN duty cycle (f_{AGN}) typically increases with M_{\star} thereby increasing $\overline{\text{BHAR}}$ (e.g., J. Aird et al. 2012; A. Bongiorno et al. 2012; T. M. Heckman & P. N. Best 2014; F. Zou et al. 2024).

X-ray surveys arguably provide the most robust constraints on SMBH growth because X-ray emission has reduced bias due to its high penetrating power and the large contrast between the X-ray emission of AGNs and stellar components (e.g., W. N. Brandt & G. Yang 2022). Recently, F. Zou et al. (2024) have obtained the best measurements of $\overline{\text{BHAR}}$ (traced by X-ray emission) utilizing the superb X-ray and multiwavelength data in nine well-studied extragalactic surveys. In this work, we quantitatively investigate the decline in SMBH growth at $z \lesssim 2$ based upon the results of F. Zou et al. (2024), and address the following key questions:

1. At $z \lesssim 2$, as redshift decreases, what causes the broad decline in SMBH growth? Is it due to (a) a shift of accretion activity to lower M_{BH} in generally lower- M_{\star} galaxies, (b) reduction in the typical λ_{Edd} at the same M_{BH} , (c) reduction in the number density of AGNs, or (d) some combination of these possibilities?
2. Why does SMBH growth decline as M_{\star} decreases? Does M_{\star} mainly modulate the typical outburst luminosity or duty cycle to reduce SMBH growth?

This paper is structured as follows. Section 2 describes the data and methodology. Sections 3.1 and 3.2 present our results for the two key questions, respectively. Section 4 summarizes this work. Throughout the paper, we adopt a flat Λ CDM cosmology with $H_0 = 70 \text{ km s}^{-1} \text{ Mpc}^{-1}$, $\Omega_{\Lambda} = 0.70$, and $\Omega_{\text{M}} = 0.30$.

We denote the $M_{\text{BH}} - M_{\star}$ relation as $M_{\text{BH}} = \eta(M_{\star})$. Most of our analyses adopt a linear relation with $\eta(M_{\star}) = 0.002 M_{\star}$ (A. Marconi et al. 2004) unless otherwise specified. This linear relation is similar to the one in A. E. Reines & M. Volonteri (2015) that is based upon dynamically measured M_{BH} . It has been shown that the $M_{\text{BH}} - M_{\star}$ relation does not have a significant redshift evolution at $z < 2$ (e.g., H. Suh et al. 2020; J. I. H. Li et al. 2023). All $M_{\text{BH}} - M_{\star}$ relations typically have ≈ 0.5 dex scatters, and our relation is appropriate in an average sense.

2. DATA AND METHODOLOGY

2.1. Data

The best current measurements of $\overline{\text{BHAR}}$ by [F. Zou et al. \(2024\)](#) utilize data from nine well-studied extragalactic surveys. These surveys follow a standard “wedding-cake” design and consist of deep, pencil-beam and shallower, wider surveys (spanning $0.05 - 60 \text{ deg}^2$), allowing us to effectively explore a wide range of parameter space. The fields include four of the Cosmic Assembly Near-infrared Deep Extragalactic Legacy Survey (CANDELS) fields, four of the Vera C. Rubin Observatory Legacy Survey of Space and Time (LSST) Deep-Drilling Fields (DDFs), and the eROSITA Final Equatorial Depth Survey (eFEDS) field. These fields have sensitive X-ray coverage and superb multiwavelength data, providing quality characterization of ≈ 8000 X-ray-selected AGNs and 1.3 million galaxies that are above the M_* -completeness limits. We summarize the information for these fields as follows:

1. CANDELS: We use the ultra-deep X-ray-to-infrared data in four of the CANDELS ([N. A. Grogin et al. 2011](#); [A. M. Koekemoer et al. 2011](#)) fields: GOODS-S, GOODS-N, Extended Groth Strip (EGS), and UKIRT Infrared Deep Sky Survey Ultra-Deep Survey (UDS). These fields have ultra-deep Chandra observations reaching megasecond depths that allow us to effectively sample AGNs at high redshift and/or low luminosity: [B. Luo et al. \(2017\)](#) for GOODS-S, [Y. Q. Xue et al. \(2016\)](#) for GOODS-N, [K. Nandra et al. \(2015\)](#) for EGS, and [D. D. Kocevski et al. \(2018\)](#) for UDS. The galaxy catalog is from [G. Yang et al. \(2019\)](#), in which the host-galaxy properties of M_* and SFR are derived using SED-fitting.
2. LSST DDFs: We use four of the LSST DDFs ([W. N. Brandt et al. 2018](#); [F. Zou et al. 2022](#)): Cosmic Evolution Survey (COSMOS), Wide Chandra Deep Field-South (W-CDF-S), European Large-Area Infrared Space Observatory Survey-S1 (ELAIS-S1), and XMM-Newton Large Scale Structure (XMM-LSS). These fields have sensitive multiwavelength data, including medium-depth X-ray coverage. The fifth LSST DDF, Euclid Deep Field-South (EDF-S), was recently selected as one of the DDFs in 2022, and it currently lacks data of comparable quality, so we did not include it. For COSMOS, Chandra provides ≈ 160 ks X-ray depth ([F. Civano et al. 2016](#)), and the galaxy properties are provided in the Appendix of [Z. Yu et al. \(2023\)](#) derived from SED-fitting. For the other three DDFs, the X-ray coverage is provided

by the XMM-Spitzer Extragalactic Representative Volume Survey (XMM-SERVS). [Q. Ni et al. \(2021\)](#) provide ≈ 30 ks XMM-Newton coverage for W-CDF-S and ELAIS-S1. [C.-T. J. Chen et al. \(2018\)](#) provide ≈ 40 ks XMM-Newton coverage for XMM-LSS. The galaxy properties of these three fields are provided by [F. Zou et al. \(2022\)](#). Note that we only focus on the regions that have both X-ray and sensitive near-infrared coverage, totaling $\approx 13 \text{ deg}^2$. We have ensured that regions with overlap with CANDELS are not double-counted.

3. eFEDS: We focus on the 60 deg^2 GAMA09 sub-field inside the full eFEDS field because its good multiwavelength coverage allows us to constrain host-galaxy properties. eFEDS has been observed by eROSITA with ≈ 2 ks depth, most sensitively at $< 2.3 \text{ keV}$. Due to the soft X-ray coverage, the X-ray properties are from [T. Liu et al. \(2022\)](#), who performed X-ray spectral analyses to account for obscuration effects. The host-galaxy properties are provided in [Z. Yu et al. \(2023\)](#).

For further information on these fields, see Section 2 of [F. Zou et al. \(2024\)](#). The wedding-cake design of the fields and their quality source characterization enabled us to sample AGNs with a wide range of rest-frame $2 - 10 \text{ keV}$ intrinsic luminosity (L_X ; $\log[L_X/\text{erg s}^{-1}] \approx 40 - 45$) across $z = 0 - 4$, so that we can capture most of the SMBH growth at $z < 4$. Particularly relevant to this work are the significantly tighter constraints set by [F. Zou et al. \(2024\)](#) upon SMBH growth at $z \lesssim 1$ for a wide range of M_* , which allow us to quantify the decline in SMBH growth accurately. This aspect is mostly enabled by the large sampled volume of the 13 deg^2 XMM-SERVS and 60 deg^2 eFEDS surveys.

To measure SMBH growth from X-ray surveys, it is necessary to correct for the obscured accretion power. This is particularly important for eFEDS, since its soft X-ray coverage can lead to a higher fraction of missed obscured AGNs, thereby introducing bias into the results. The correction utilizes the detection probability of our X-ray surveys to correct for the obscured accretion power, which is calibrated based upon the well-determined $\log N - \log S$ relation, the expected surface number density per unit X-ray flux with the detection procedures deconvolved (see Section 3.1.1 of [F. Zou et al. 2024](#)). Thus, the measurements have been corrected for all of the missed obscured Compton-thin (CN) AGNs and for part of the missed Compton-thick (CT) AGNs in our fields. [F. Zou et al. \(2024\)](#) showed that excluding eFEDS from the analyses leads to differences in $\overline{\text{BHAR}}$ smaller than the 1σ statistical uncertainties.

We have further verified in Appendix A that the median values of our results remain consistent when eFEDS is excluded. Importantly, we do not rely solely on eFEDS to probe SMBH growth at low redshift and/or high luminosity, as the $\approx 13 \text{ deg}^2$ area in the LSST DDFs with sensitive X-ray coverage above 2 keV already provides meaningful constraints. eFEDS increases the number of our X-ray AGNs at $z \lesssim 1$ by $\approx 60\%$ and thereby reduces statistical uncertainties, allowing more accurate measurements of the SMBH growth decline since $z \approx 2$.

One systematic uncertainty arises from the fact that correcting for CT accretion is generally difficult for our fields, particularly for eFEDS due to its soft X-ray coverage. However, the missing CT accretion should not have a material impact on our results for two reasons. First, some CT AGNs can still be detected by Chandra or XMM-Newton (e.g., J. Li et al. 2020; W. Yan et al. 2023), particularly since increasing redshift allows us to probe up to rest-frame 10–25 keV at $z < 2$ with greater penetrating power. Second, using the X-ray luminosity function (XLF) with the column-density distribution from Sections 3 and 6 of Y. Ueda et al. (2014), F. Zou et al. (2024) found that the fractional accretion power at column densities above 10^{24} cm^{-2} is $\approx 38\%$ across all redshifts; similarly, J. Buchner et al. (2015) showed that the X-ray luminosity density at $\log[L_X/\text{erg s}^{-1}] > 43.2$ contributed by CT AGNs is $\approx 35\text{--}45\%$ at $z = 0.8\text{--}3.6$. Thus, the systematic bias upon SMBH growth from potentially missed CT accretion is $\lesssim 0.2 \text{ dex}$, with the 0.2 dex upper limit corresponding to the extreme case in which all of the $\approx 40\%$ CT accretion power is missed.⁹ This $\lesssim 0.2 \text{ dex}$ bias arises solely from possible missed CT accretion after applying the obscuration correction of F. Zou et al. (2024), and is not specifically attributed to eFEDS.

2.2. Methodology

We denote $p(\lambda|M_*, z)$ and $p(\lambda_{\text{Edd}}|M_*, z)$ as the conditional probability density per unit $\log \lambda$ and $\log \lambda_{\text{Edd}}$ of a galaxy with (M_*, z) hosting an AGN with $\lambda \equiv L_X/M_* / [\text{erg s}^{-1} M_\odot^{-1}]$ and $\lambda_{\text{Edd}} \equiv L_{\text{bol}}/L_{\text{Edd}}$, respectively, where L_{bol} is the AGN bolometric luminosity and L_{Edd} is the Eddington luminosity of the SMBH. F. Zou et al. (2024) obtained $p(\lambda|M_*, z)$ at $z = 0\text{--}4$ with $\log M_* = 9.5\text{--}12$, reaching down to $\log \lambda > 31.5$. The X-ray bolometric correction factor as a function of L_{bol} (in units of erg s^{-1}) is $k_X(L_{\text{bol}})$. For a fixed M_* , by

definition,

$$\begin{aligned} p(\lambda_{\text{Edd}}|M_*, z) &= p(\lambda|M_*, z) \frac{d \log \lambda}{d \log \lambda_{\text{Edd}}} \\ &= p(\lambda|M_*, z) \left(1 - \frac{d \log k_X(L_{\text{bol}})}{d \log L_{\text{bol}}} \right). \end{aligned} \quad (1)$$

The second equality holds because

$$\begin{aligned} \lambda_{\text{Edd}} &= \frac{L_X k_X(L_{\text{bol}})}{1.26 \times 10^{38} \times M_{\text{BH}}} = \frac{L_X k_X(L_{\text{bol}}) M_*}{1.26 \times 10^{38} \times \eta(M_*) M_*} \\ &= \lambda k_X(L_{\text{bol}}) \frac{M_*}{1.26 \times 10^{38} \times \eta(M_*)}. \end{aligned} \quad (2)$$

The M_* -related term is constant when we calculate $p(\lambda_{\text{Edd}}|M_*, z)$. We take the logarithm of both sides of Equation 2, and differentiate both sides with respect to $\log \lambda_{\text{Edd}}$. Since $d \log \lambda_{\text{Edd}} = d \log L_{\text{bol}}$ when $\eta(M_*)$ is fixed, we have

$$\frac{d \log \lambda}{d \log \lambda_{\text{Edd}}} = 1 - \frac{d \log k_X(L_{\text{bol}})}{d \log L_{\text{bol}}}. \quad (3)$$

We adopt the $\log k_X - \log L_{\text{bol}}$ relation from Equation 2 of F. Duras et al. (2020):

$$k_X = 10.96 \left[1 + \left(\frac{\log[L_{\text{bol}}/L_\odot]}{11.93} \right)^{17.79} \right]. \quad (4)$$

k_X diverges at very high L_{bol} , so we set an upper limit of $k_X = 100$ because this is about the maximum value observed in previous literature (e.g., A. Marconi et al. 2004; P. F. Hopkins et al. 2007; R. V. Vasudevan & A. C. Fabian 2007). The limit corresponds to large L_{bol} and L_X thresholds of $\log[L_{\text{bol}}/\text{erg s}^{-1}] = 47.0$ and $\log[L_X/\text{erg s}^{-1}] = 45.0$. For L_{bol} higher than the threshold L_{bol} , we apply a constant $k_X = 100$. Although higher k_X has been observed for very luminous quasars (e.g., S. Martocchia et al. 2017), these quasars are very rare and are generally missed in our fields. We have tested that setting the upper limit of k_X to ≈ 400 only changes our results for the highest λ_{Edd} bin (Section 3.1) by $< 0.2 \text{ dex}$.

With $p(\lambda_{\text{Edd}}|M_*, z)$ [or equivalently, $p(\lambda|M_*, z)$], we can derive many metrics describing SMBH growth. For example, one of the key results in F. Zou et al. (2024) is the measurement of $\overline{\text{BHAR}}$, sampled down to AGNs with $\lambda_{\text{Edd}} = 0.0013$ (corresponding to $\log \lambda = 31.5$). We adopt a radiative efficiency of $\epsilon = 0.1$, which is a typical value for the general AGN population. Although at $\lambda_{\text{Edd}} \lesssim 0.01$, radiatively inefficient accretion flows (RIAFs) may become relevant, they are not expected to contribute a significant fraction of SMBH growth (e.g., R. Narayan & I. Yi 1995; F. Yuan & R. Narayan 2014).

⁹ The $\approx 0.2 \text{ dex}$ systematic bias has been estimated by assuming that we could only detect the $\approx 60\%$ contribution from CN accretion: $\log(0.6) = -0.22 \text{ dex}$.

In fact, we have checked that if we only focus on AGNs with $\lambda_{\text{Edd}} > 0.01$, our results are not materially different. For SMBHs accreting between $\lambda_{\text{Edd}}^{\text{low}}$ and $\lambda_{\text{Edd}}^{\text{high}}$, $\overline{\text{BHAR}}$ can be expressed as

$$\begin{aligned} \overline{\text{BHAR}}(M_*, z; \lambda_{\text{Edd}}^{\text{low}}, \lambda_{\text{Edd}}^{\text{high}}) \\ = \int_{\log \lambda_{\text{Edd}}^{\text{low}}}^{\log \lambda_{\text{Edd}}^{\text{high}}} \frac{(1 - \epsilon) \lambda_{\text{Edd}} M_* \kappa(M_*)}{\epsilon c^2} p(\lambda_{\text{Edd}} | M_*, z) d \log \lambda_{\text{Edd}}, \end{aligned} \quad (5)$$

where

$$\kappa(M_*) = [1.26 \times 10^{38} \times \eta(M_*) / M_*] \text{ erg s}^{-1} M_{\odot}^{-1}, \quad (6)$$

which converts $\lambda_{\text{Edd}} M_*$ to L_{bol} . For most of our analyses, under the assumption of $\eta(M_*) \equiv M_{\text{BH}} = 0.002 M_*$, $\kappa(M_*)$ is constant. However, we retain the notation in Equation 6 because it is applicable for other nonlinear $M_{\text{BH}} - M_*$ relations (e.g., A. E. Reines & M. Volonteri 2015; J. E. Greene et al. 2020). It is worth noting that $\overline{\text{BHAR}}$ represents the actual *growth rate* of SMBHs rather than the mass accretion rate at a certain radius from the SMBH. In the following Section, we will derive other quantities of interest using $p(\lambda_{\text{Edd}} | M_*, z)$, including ρ_{BHAR} and n_{AGN} , to answer our key questions in Section 1. We derive the statistical uncertainties of our results using a Monte Carlo method. F. Zou et al. (2024) obtained 10,000 posterior samples of $p(\lambda | M_*, z)$ with a Hamiltonian Monte Carlo sampler, adopting parameter priors described in Section 3.1.3 of their work. From these posterior samples, we randomly select 1000 samples without replacement and repeat our analyses (Section 3) 1000 times to estimate the statistical uncertainties. We do not consider additional sources of uncertainty beyond $p(\lambda | M_*, z)$ (e.g., k_X , $M_{\text{BH}} - M_*$ relation). While this approach does not affect the median values of our results, it may introduce an additional uncertainty of $\approx 0.2 - 0.3$ dex. Unless otherwise specified, all quoted statistical uncertainties correspond to 90% confidence intervals.

3. RESULTS

3.1. What Primarily Causes the Decline in SMBH Growth as a Function of Redshift?

In this subsection, we investigate the reason why ρ_{BHAR} declines dramatically at $z \lesssim 1.5 - 2$. As a useful first-order approximation, ρ_{BHAR} can be factored into three redshift-dependent components and a constant factor:

$$\rho_{\text{BHAR}} = n_{\text{AGN}}^{\text{eff}} \times \langle \lambda_{\text{Edd}} \rangle \times \langle M_{\text{BH}} \rangle \times \frac{(1 - \epsilon) \times 1.26 \times 10^{38}}{\epsilon c^2}, \quad (7)$$

where $\langle \lambda_{\text{Edd}} \rangle$ and $\langle M_{\text{BH}} \rangle$ represent the typical λ_{Edd} and typical M_{BH} of AGNs that contribute to most of ρ_{BHAR} . Note that $1.26 \times 10^{38} \langle M_{\text{BH}} \rangle = \langle M_* \kappa(M_*) \rangle$. The last three terms on the right-hand side of Equation 7, $\langle \lambda_{\text{Edd}} \rangle \langle M_{\text{BH}} \rangle (1 - \epsilon) / \epsilon c^2 \times 1.26 \times 10^{38}$, simply describe the typical SMBH accretion rate *per AGN*. $n_{\text{AGN}}^{\text{eff}}$ is the “effective” AGN number density set as if all AGNs have the same SMBH mass of $\langle M_{\text{BH}} \rangle$ and accrete at $\langle \lambda_{\text{Edd}} \rangle$ in order to produce the observed ρ_{BHAR} . $n_{\text{AGN}}^{\text{eff}}$, $\langle \lambda_{\text{Edd}} \rangle$, and $\langle M_{\text{BH}} \rangle$ correspond to the three redshift-dependent factors that control the decline in SMBH growth in key question 1 in Section 1. While $\langle \lambda_{\text{Edd}} \rangle$ and $\langle M_{\text{BH}} \rangle$ represent the properties of a typical AGN, $n_{\text{AGN}}^{\text{eff}}$ is useful in assessing the expected number density of those AGNs. By definition, $n_{\text{AGN}}^{\text{eff}}$ should only be calculated using Equation 7 after ρ_{BHAR} , $\langle \lambda_{\text{Edd}} \rangle$, and $\langle M_{\text{BH}} \rangle$ are determined. Note that $n_{\text{AGN}}^{\text{eff}}$ may be different from the true AGN number density n_{AGN} , because $\langle \lambda_{\text{Edd}} \rangle$ and $\langle M_{\text{BH}} \rangle$ are not the arithmetic average of λ_{Edd} and M_* for all AGNs. We will further illustrate this point in Section 3.1.2. In the following subsections, we aim to measure ρ_{BHAR} , $\langle \lambda_{\text{Edd}} \rangle$, $\langle M_{\text{BH}} \rangle$, and $n_{\text{AGN}}^{\text{eff}}$ in different redshift bins. The redshift bins are based upon those in J. R. Weaver et al. (2023), with bin boundaries at 0.2, 0.5, 0.8, 1.1, 1.5, 2.0, 2.5, 3.0, 3.5, and 4.0 (i.e., this is the binning available for the galaxy stellar mass function; see Section 3.1.1). The numbers of X-ray AGNs and normal galaxies are summarized at the bottom of Table 1. We also aim to quantify the impact of these factors on the decline of ρ_{BHAR} , i.e.,

$$\Delta \log \rho_{\text{BHAR}} = \Delta \log n_{\text{AGN}}^{\text{eff}} + \Delta \log \langle \lambda_{\text{Edd}} \rangle + \Delta \log \langle M_{\text{BH}} \rangle, \quad (8)$$

where the Δ ’s represent the change of these quantities from the $z = 1.5 - 2$ bin to $z = 0.2 - 0.5$ bin.

3.1.1. Cosmic BHAR Density and AGN Number Density

We can calculate ρ_{BHAR} in a redshift bin for SMBHs accreting between $\lambda_{\text{Edd}}^{\text{low}}$ and $\lambda_{\text{Edd}}^{\text{high}}$ by convolving $\overline{\text{BHAR}}$ with the galaxy stellar mass function (SMF; ϕ_M) in that redshift bin:

$$\begin{aligned}
\rho_{\text{BHAR}}(z; \lambda_{\text{Edd}}^{\text{low}}, \lambda_{\text{Edd}}^{\text{high}}) &= \int_{9.5}^{12} \overline{\text{BHAR}}(M_*, z; \lambda_{\text{Edd}}^{\text{low}}, \lambda_{\text{Edd}}^{\text{high}}) \phi_{\text{M}}(M_*|z) d \log M_* \\
&= \int_{9.5}^{12} \int_{\log \lambda_{\text{Edd}}^{\text{low}}}^{\log \lambda_{\text{Edd}}^{\text{high}}} \frac{(1-\epsilon)p(\lambda_{\text{Edd}}|M_*, z)\phi_{\text{M}}(M_*|z)}{\epsilon c^2} \\
&\quad \times \lambda_{\text{Edd}} M_* \kappa(M_*) d \log \lambda_{\text{Edd}} d \log M_* \\
&= \frac{1-\epsilon}{\epsilon c^2} \int_{9.5}^{12} \int_{\log \lambda_{\text{Edd}}^{\text{low}}}^{\log \lambda_{\text{Edd}}^{\text{high}}} f(\lambda_{\text{Edd}}, M_*|z) \\
&\quad \times \lambda_{\text{Edd}} M_* \kappa(M_*) d \log \lambda_{\text{Edd}} d \log M_*, \tag{9}
\end{aligned}$$

where

$$f(\lambda_{\text{Edd}}, M_*|z) \equiv p(\lambda_{\text{Edd}}|M_*, z)\phi_{\text{M}}(M_*|z), \tag{10}$$

We adopt the SMF from [J. R. Weaver et al. \(2023\)](#), using the same redshift bins as defined in their work. Our analyses only consider SMBHs residing in galaxies with $\log M_* = 9.5 - 12$ because the BHAR for massive black holes in dwarf galaxies is still poorly understood, and dwarf galaxies do not necessarily always host massive black holes (e.g., [B. P. Miller et al. 2015](#); [E. Gallo & A. Sesana 2019](#); [F. Zou et al. 2025](#)).

The top panel of Figure 1 displays ρ_{BHAR} for AGNs in different λ_{Edd} bins as functions of redshift. For the total ρ_{BHAR} sampled by all of our AGNs, we successfully produce the peak at $z \approx 1.5 - 2$, and the decline of ρ_{BHAR} from $z = 1.5 - 2$ to $z = 0.2 - 0.5$ is $-1.28^{+0.08}_{-0.08}$ dex. In Appendix B, we present simple functional fits to our measurements in different λ_{Edd} bins. For comparison, in Figure 1 we present the cosmic star-formation rate density (SFRD) from [P. Madau & M. Dickinson \(2014\)](#), which is scaled by a factor of 5000 to approximately match the peak of total ρ_{BHAR} . The decline in ρ_{BHAR} is larger than the decline in SFRD, which is consistent with previous results (e.g., [J. Aird et al. 2015](#); [G. Yang et al. 2023](#)). We also show the total ρ_{BHAR} from [Y. Ueda et al. \(2014\)](#) and [G. Yang et al. \(2018\)](#). Our results are generally in agreement with theirs except at $z < 0.8$ where our total ρ_{BHAR} is slightly lower than that in [Y. Ueda et al. \(2014\)](#). This may be because [Y. Ueda et al. \(2014\)](#) adopted the X-ray bolometric correction in [P. F. Hopkins et al. \(2007\)](#), which is slightly larger than that in [F. Duras et al. \(2020\)](#) at $\log L_X = 42 - 45$.

Our results also show AGN downsizing in different λ_{Edd} bins instead of the typical downsizing phenomena observed in different luminosity bins. We find that ρ_{BHAR} contributed by high- λ_{Edd} AGNs peaks at a higher redshift than for low- λ_{Edd} AGNs. The bot-

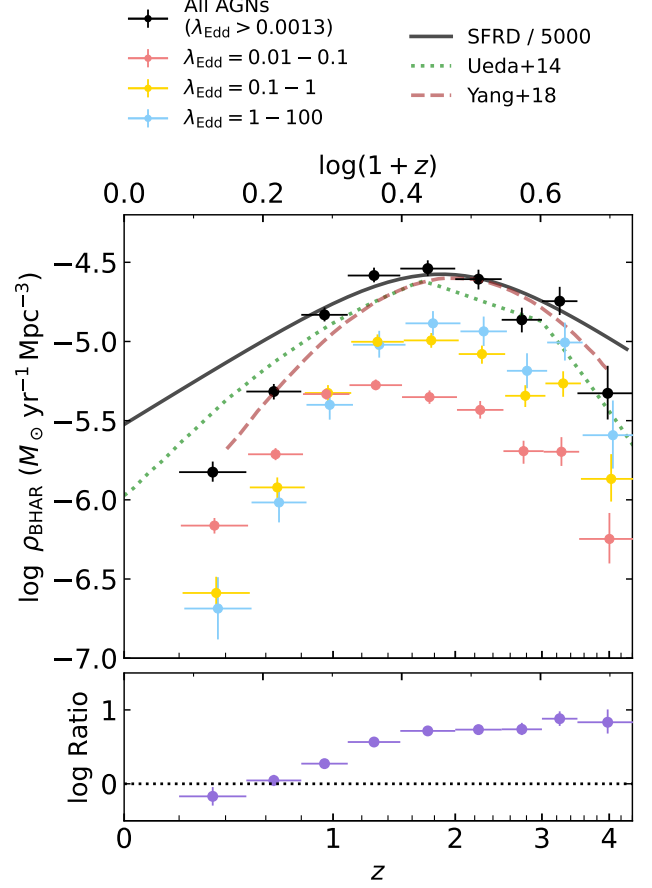


Figure 1. Top panel: ρ_{BHAR} as a function of redshift. The black data points represent the total ρ_{BHAR} sampled by our data. The red, yellow, and blue data points represent ρ_{BHAR} for AGNs accreting at $\lambda_{\text{Edd}} = 0.01 - 0.1$, $\lambda_{\text{Edd}} = 0.1 - 1$, and $\lambda_{\text{Edd}} = 1 - 100$, respectively. For comparison, the cosmic SFRD ([P. Madau & M. Dickinson 2014](#)) scaled by a factor of 5000 is shown as the dashed line to approximately match the peak of ρ_{BHAR} at $z \approx 2$. The green dotted line and the brown dashed line represent the total ρ_{BHAR} from [Y. Ueda et al. \(2014\)](#) and [G. Yang et al. \(2018\)](#), respectively. Bottom panel: logarithm of the ratio of ρ_{BHAR} contributed by AGNs with $\lambda_{\text{Edd}} > 0.1$ to that contributed by AGNs with $\lambda_{\text{Edd}} < 0.1$. The error bars represent the 90% confidence intervals derived with our Monte Carlo method.

tom panel of Figure 1 shows the ratio of ρ_{BHAR} contributed by AGNs with $\lambda_{\text{Edd}} > 0.1$ to that by AGNs with $\lambda_{\text{Edd}} < 0.1$. At $z \gtrsim 1$, ρ_{BHAR} is mainly contributed by high- λ_{Edd} AGNs. Our results also indicate that super-Eddington accretion contributes to much of the accretion density at $z \gtrsim 2$, but the difference is not very significant and may suffer additional bias. This is because the difference between the $\lambda_{\text{Edd}} = 0.1 - 1$ bin and $\lambda_{\text{Edd}} = 1 - 100$ bin is generally comparable to the 90% statistical uncertainty, and at $z > 3$, there may be more hidden accretion power at low- λ_{Edd} than ex-

pected (see the discussion at the end of Section 3.1.2). At $z \lesssim 0.5$, more of the accretion activity has shifted to low- λ_{Edd} AGNs, and about half of the ρ_{BHAR} at $z = 0.2 - 0.5$ is contributed by AGNs with $\lambda_{\text{Edd}} < 0.1$. We have also verified that our result for super-Eddington AGNs is not sensitive to the choice of $\lambda_{\text{Edd}}^{\text{high}}$. The results are very similar when $\lambda_{\text{Edd}}^{\text{high}}$ takes any value > 100 ; the difference is $\lesssim 0.15$ dex when we change $\lambda_{\text{Edd}}^{\text{high}}$ from 100 to 10. This difference is also smaller than the 90% statistical uncertainty for the $\lambda_{\text{Edd}} = 1 - 100$ bin. So far, we have not yet quantified the decline in $\langle \lambda_{\text{Edd}} \rangle$, but the fact that the primary contributor to ρ_{BHAR} shifts from AGNs with $\lambda_{\text{Edd}} > 0.1$ to those with $\lambda_{\text{Edd}} < 0.1$ indicates that $\langle \lambda_{\text{Edd}} \rangle$ has declined significantly from $z \approx 2$ to $z \approx 0.2$. We have verified that the results for ρ_{BHAR} remain similar after excluding eFEDS from our analyses in Appendix A.

Similar to the calculation of ρ_{BHAR} , the AGN host-galaxy SMF ($\phi_{\text{M}}^{\text{AGN}}$) for AGNs accreting between $\lambda_{\text{Edd}}^{\text{low}}$ and $\lambda_{\text{Edd}}^{\text{high}}$ can be directly calculated by convolving $p(\lambda_{\text{Edd}}|M_*, z)$ with ϕ_{M} :

$$\begin{aligned} \phi_{\text{M}}^{\text{AGN}}(M_*; \lambda_{\text{Edd}}^{\text{low}}, \lambda_{\text{Edd}}^{\text{high}}|z) &= \int_{\log \lambda_{\text{Edd}}^{\text{low}}}^{\log \lambda_{\text{Edd}}^{\text{high}}} p(\lambda_{\text{Edd}}|M_*, z) \phi_{\text{M}}(M_*|z) d \log \lambda_{\text{Edd}} \\ &= \int_{\log \lambda_{\text{Edd}}^{\text{low}}}^{\log \lambda_{\text{Edd}}^{\text{high}}} f(\lambda_{\text{Edd}}, M_*|z) d \log \lambda_{\text{Edd}}. \end{aligned} \quad (11)$$

The $\phi_{\text{M}}^{\text{AGN}}$ at $z < 2.0$ in different λ_{Edd} bins is shown in Figure 2. From $z = 1.5 - 2.0$ to $z = 0.2 - 0.5$, the decline in $\phi_{\text{M}}^{\text{AGN}}$ is most significant in the $\lambda_{\text{Edd}} = 1 - 100$ bin, reaching ≈ 2 dex at $\log M_* = 10 - 11.5$, while the decline in the $\lambda_{\text{Edd}} = 0.01 - 0.1$ bin is only < 1 dex at all M_* . The result is consistent with that in Figure 1, where ρ_{BHAR} for high- λ_{Edd} AGNs declines more significantly than that for low- λ_{Edd} AGNs.

With $\phi_{\text{M}}^{\text{AGN}}$ we can then further derive n_{AGN} for AGNs accreting between $\lambda_{\text{Edd}}^{\text{low}}$ and $\lambda_{\text{Edd}}^{\text{high}}$ as

$$\begin{aligned} n_{\text{AGN}}(z; \lambda_{\text{Edd}}^{\text{low}}, \lambda_{\text{Edd}}^{\text{high}}) &= \int_{9.5}^{12} \phi_{\text{M}}^{\text{AGN}}(M_*; \lambda_{\text{Edd}}^{\text{low}}, \lambda_{\text{Edd}}^{\text{high}}|z) d \log M_*. \end{aligned} \quad (12)$$

Note that Equation 12 is not intended to calculate $n_{\text{AGN}}^{\text{eff}}$, because by definition, after quantifying $\langle \lambda_{\text{Edd}} \rangle$ and $\langle M_{\text{BH}} \rangle$, $n_{\text{AGN}}^{\text{eff}}$ is obtained using Equation 7. However, Equation 12 can still provide insights into how many AGNs have λ_{Edd} and M_{BH} similar to $\langle \lambda_{\text{Edd}} \rangle$ and $\langle M_{\text{BH}} \rangle$. In the next subsection, we will first quantify $\langle \lambda_{\text{Edd}} \rangle$ and $\langle M_{\text{BH}} \rangle$. With them, we can further determine $n_{\text{AGN}}^{\text{eff}}$.

3.1.2. Quantifying the Impact of $\langle \lambda_{\text{Edd}} \rangle$, $\langle M_{\text{BH}} \rangle$, and $n_{\text{AGN}}^{\text{eff}}$

The quantities $\langle \lambda_{\text{Edd}} \rangle$ and $\langle M_{\text{BH}} \rangle$ are less well-defined than ρ_{BHAR} and n_{AGN} . Since we expect $\langle \lambda_{\text{Edd}} \rangle$ and $\langle M_{\text{BH}} \rangle$ can represent the λ_{Edd} and M_{BH} of the AGNs that contribute to most of ρ_{BHAR} , we can determine $\langle \lambda_{\text{Edd}} \rangle$ and $\langle M_{\text{BH}} \rangle$ by examining the contribution to ρ_{BHAR} in different $(\log \lambda_{\text{Edd}}, \log M_{\text{BH}})$ grid cells in the $\log \lambda_{\text{Edd}} - \log M_{\text{BH}}$ plane and identifying the region that produces most of the contribution.

From Equations 10, 11, and 12, we denote $F(\lambda_{\text{Edd}}, M_*|z)$ as the conditional probability density per unit $\log \lambda_{\text{Edd}}$ per unit $\log M_*$ that a galaxy at z has M_* and hosts a SMBH accreting at λ_{Edd} :

$$\begin{aligned} F(\lambda_{\text{Edd}}, M_*|z) &= \frac{f(\lambda_{\text{Edd}}, M_*|z)}{\iint f(\lambda_{\text{Edd}}, M_*|z) d \log \lambda_{\text{Edd}} d \log M_*} \\ &= \frac{f(\lambda_{\text{Edd}}, M_*|z)}{n_{\text{AGN}}(z)}. \end{aligned} \quad (13)$$

The quantity $(1 - \epsilon)/(\epsilon c^2) \times F(\lambda_{\text{Edd}}, M_*|z) \times M_* \lambda_{\text{Edd}} \kappa(M_*)$ provides a measure of the contribution to ρ_{BHAR} per galaxy at different $\log \lambda_{\text{Edd}}$ and $\log M_{\text{BH}}$ in the $\log \lambda_{\text{Edd}} - \log M_{\text{BH}}$ plane after we convert M_* to M_{BH} based upon the adopted $M_{\text{BH}} - M_*$ relation. Note that the integration in Equation 13 is for galaxies with $\log M_* = 9.5 - 12$. Figure 3 shows the results assuming the median $p(\lambda_{\text{Edd}}|M_*, z)$, with the integration range of $\log \lambda_{\text{Edd}}$ restricted between -3 and 2 . We define $\log \langle \lambda_{\text{Edd}} \rangle$ and $\log \langle M_{\text{BH}} \rangle$ such that they are represented by the intersection point of the running median of $\log \lambda_{\text{Edd}}$ and $\log M_{\text{BH}}$ in the $\log \lambda_{\text{Edd}} - \log M_{\text{BH}}$ plane. The solid error bars represent the regions that are enclosed by the 25 - 75% quantiles of λ_{Edd} and M_{BH} . Those regions are generally consistent with the maximum values of the heatmaps at all redshifts, indicating our identification of $\langle \lambda_{\text{Edd}} \rangle$ and $\langle M_{\text{BH}} \rangle$ can truly represent the AGNs that contribute most of ρ_{BHAR} .

We further present the evolution of $\langle \lambda_{\text{Edd}} \rangle$ and $\langle M_{\text{BH}} \rangle$ at different redshifts in Figure 4. The error bars in the top panel are the same as those in Figure 3, while those in the bottom panel represent the 90% confidence intervals derived with our Monte Carlo method. From Figure 4, we can directly quantify the change in $\langle \lambda_{\text{Edd}} \rangle$ and $\langle M_{\text{BH}} \rangle$. At $z = 1.5 - 2.5$, $\log \langle \lambda_{\text{Edd}} \rangle$ is between about -0.7 and 0.4 , indicating most of the accretion power is from near-Eddington or super-Eddington AGNs. As redshift decreases, $\langle \lambda_{\text{Edd}} \rangle$ decreases significantly with $\Delta \log \langle \lambda_{\text{Edd}} \rangle = -1.35^{+0.46}_{-0.39}$ dex while $\langle M_{\text{BH}} \rangle$ only slightly

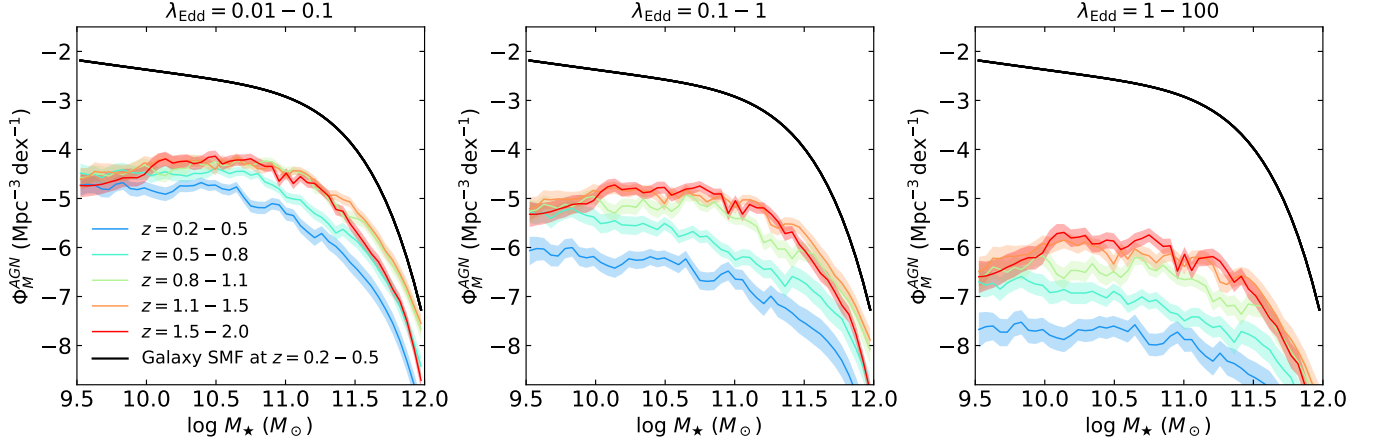


Figure 2. AGN host-galaxy SMF ϕ_M^{AGN} at different redshifts, with colors defined in the legend. The left, middle, and right panels show the $\lambda_{\text{Edd}} = 0.01 - 0.1$, $\lambda_{\text{Edd}} = 0.1 - 1$, and $\lambda_{\text{Edd}} = 1 - 100$ bins, respectively. For comparison, the galaxy SMF at $z = 0.2 - 0.5$ in J. R. Weaver et al. (2023) is shown as black solid curves. The colored shaded stripes represent the 1σ uncertainty from $p(\lambda_{\text{Edd}}|M_\star, z)$.

decreases by $0.21^{+0.11}_{-0.11}$ dex.¹⁰ By $z = 0.2$, $\log\langle\lambda_{\text{Edd}}\rangle$ is less than -1.0 . These trends are consistent with the ρ_{BHAR} evolution shown in Figure 1, where high- λ_{Edd} AGNs dominate most ρ_{BHAR} at $z \gtrsim 1.5$, while low- λ_{Edd} AGNs gradually dominate toward lower redshift.

So far, we have quantified ρ_{BHAR} , $\langle\lambda_{\text{Edd}}\rangle$, and $\langle M_{\text{BH}}\rangle$ at different redshifts. We now use Equation 7 to calculate $n_{\text{AGN}}^{\text{eff}}$, and use Equation 12 to calculate n_{AGN} in different λ_{Edd} bins. The results are shown in Figure 5. We provide simple functional fits to our n_{AGN} measurements in different λ_{Edd} bins in Appendix B. For comparison, in Figure 5 we show the total n_{AGN} for AGNs with $\log L_X > 42$ from J. Buchner et al. (2015), T. Miyaji et al. (2015), and A. Peca et al. (2023). Our results generally agree with those in the literature. n_{AGN} declines at all λ_{Edd} from $z \approx 2$ to $z \approx 0.2$, and AGNs with low- λ_{Edd} ($\lambda_{\text{Edd}} < 0.1$) always dominate the total n_{AGN} at $z < 4$. The decline is most significant in the $\lambda_{\text{Edd}} = 1 - 100$ bin, reaching ≈ 1.6 dex from $z = 1.5 - 2.0$ to $z = 0.2 - 0.5$, and the decline in lower- λ_{Edd} bins is much smaller, which is consistent with the evolution of ϕ_M^{AGN} shown in Figure 2. The decline in total n_{AGN} is mostly due to the general decline in λ_{Edd} , where AGNs accreting slightly higher than our sample limit ($\lambda_{\text{Edd}} > 0.0013$) are shifted below the limit. We have also verified that n_{AGN} remain similar after excluding eFEDS from our analyses in Appendix A. However, $n_{\text{AGN}}^{\text{eff}}$ shows dramatically different behavior. From $z = 4$ to $z \approx 0.5$, $n_{\text{AGN}}^{\text{eff}}$ is consistently increasing, and it

only shows flattening or a slight downward trend in the last redshift bin of $z = 0.2 - 0.5$. The increase of $n_{\text{AGN}}^{\text{eff}}$ from $z = 1.5 - 2.0$ to $z = 0.2 - 0.5$ is $0.29^{+0.38}_{-0.46}$ dex.¹¹ Although the increase is not significant considering its 90% statistical uncertainty, this result can be understood by the drastic decrease in $\langle\lambda_{\text{Edd}}\rangle$ shown in Figure 4. As $\langle\lambda_{\text{Edd}}\rangle$ decreases, the main contributor to ρ_{BHAR} is gradually shifted to low- λ_{Edd} AGNs that always dominate the total n_{AGN} , but since the total n_{AGN} decreases, $n_{\text{AGN}}^{\text{eff}}$ is generally constant from $z = 1.5 - 2.0$ to $z = 0.2 - 0.5$. Figure 5 also demonstrates that $n_{\text{AGN}}^{\text{eff}}$ is different from the total n_{AGN} . Take the $z = 1.5 - 2$ bin as an example: $\log\langle\lambda_{\text{Edd}}\rangle$ is about between -0.7 and 0.2 in Figure 4, which indicates ρ_{BHAR} is hardly contributed to by AGNs at the other λ_{Edd} values. Thus $n_{\text{AGN}}^{\text{eff}}$ is similar to n_{AGN} in the $\lambda_{\text{Edd}} = 0.1 - 1$ bin (as shown in Figure 5) and hardly counts AGNs in the other λ_{Edd} bins. We also calculate the expected n_{AGN} for AGNs within the 25–75% quantile of λ_{Edd} (i.e., for AGNs with $\langle\lambda_{\text{Edd}}\rangle$). The estimates for $n_{\text{AGN}}^{\text{eff}}$ and n_{AGN} for AGNs with $\langle\lambda_{\text{Edd}}\rangle$ are generally consistent within the 90% statistical uncertainty, indicating that our estimated $\langle\lambda_{\text{Edd}}\rangle$ can truly represent the typical λ_{Edd} .

We summarize our results in Table 1. We also test the $M_{\text{BH}} - M_\star$ relation in J. E. Greene et al. (2020), which is nonlinear with $M_{\text{BH}} \propto M_\star^{1.61}$. The results are generally similar to those assuming $M_{\text{BH}} = 0.002 M_\star$.

From our analyses above, we have shown that the decline in $\langle\lambda_{\text{Edd}}\rangle$ is the primary driver of the broad decline in ρ_{BHAR} . The contribution from

¹⁰ $\Delta \log\langle\lambda_{\text{Edd}}\rangle = -1.35^{+0.27}_{-0.25}$ dex and $\Delta \log\langle M_{\text{BH}}\rangle = -0.21^{+0.06}_{-0.06}$ dex when considering the 68% statistical uncertainty.

¹¹ $\Delta \log n_{\text{AGN}}^{\text{eff}} = 0.29^{+0.25}_{-0.27}$ dex when considering the 68% uncertainty.

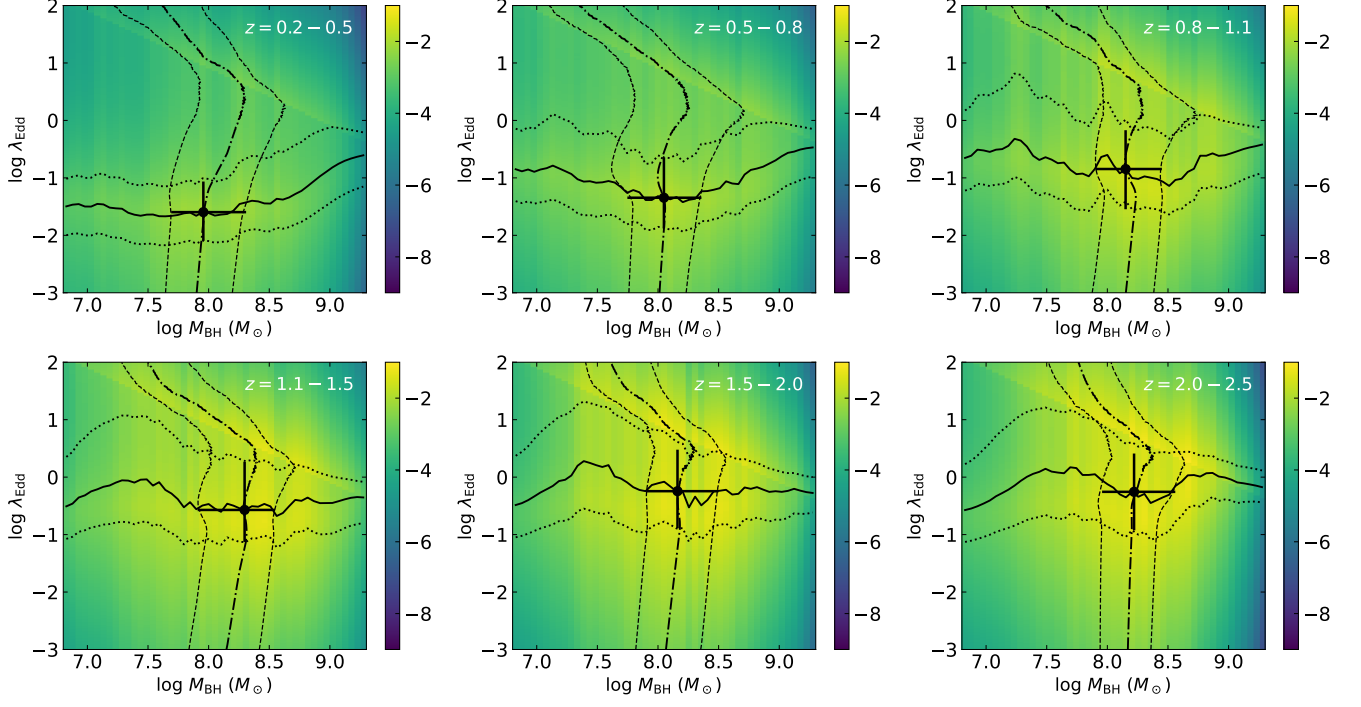


Figure 3. Contribution to ρ_{BHAR} per galaxy at different redshifts assuming the median $p(\lambda_{\text{Edd}}|M_*, z)$ and $M_{\text{BH}} = 0.002M_*$. The color bars represent the logarithm of $(1-\epsilon)/(\epsilon c^2) \times F(\lambda_{\text{Edd}}, M_*|z) \times M_* \lambda_{\text{Edd}} \kappa(M_*)$. The median values of $\log \lambda_{\text{Edd}}$ ($\log M_{\text{BH}}$) at fixed $\log M_{\text{BH}}$ ($\log \lambda_{\text{Edd}}$) are shown as solid (dash-dotted) curves. The 25 – 75% quantiles of $\log \lambda_{\text{Edd}}$ ($\log M_{\text{BH}}$) at fixed $\log M_{\text{BH}}$ ($\log \lambda_{\text{Edd}}$) are shown as dotted (dashed) curves. The error bars represent the $\log \langle \lambda_{\text{Edd}} \rangle$ and $\log \langle M_{\text{BH}} \rangle$ that roughly span the region enclosed by the 25 – 75% quantiles of $\log \lambda_{\text{Edd}}$ and $\log M_{\text{BH}}$.

$\langle M_{\text{BH}} \rangle$ ($\Delta \log \langle M_{\text{BH}} \rangle = -0.21^{+0.11}_{-0.11}$ dex) is about 13 times smaller than that from $\langle \lambda_{\text{Edd}} \rangle$ ($\Delta \log \langle \lambda_{\text{Edd}} \rangle = -1.35^{+0.46}_{-0.39}$ dex). On the other hand, although n_{AGN} for AGNs in all λ_{Edd} bins drops significantly, $n_{\text{AGN}}^{\text{eff}}$ increases because it is driven by the decline in $\langle \lambda_{\text{Edd}} \rangle$. Our results are also generally consistent with and extend those in K. Nandra et al. (2025), where they compare the low-redshift (median $z = 0.34$) eFEDS hard X-ray selected AGNs with the higher-redshift sample from the Chandra COSMOS legacy survey of H. Suh et al. (2020) (median $z = 1.58$). These two samples have similar M_{BH} distributions and luminosity limits at their median redshifts, but the eFEDS low-redshift sample has significantly lower median λ_{Edd} , indicating the decline in global accretion rate is primarily due to a reduction in the typical λ_{Edd} , rather than a shift of accretion to lower-mass SMBHs.

Our analyses assume no significant redshift evolution in the $M_{\text{BH}} - M_*$ relation at $z < 2$ as supported by the recent studies of, e.g., H. Suh et al. (2020) and J. I. H. Li et al. (2023). However, some earlier studies report an increasing M_{BH}/M_* ratio toward higher redshift (≈ 0.3 dex from $z \approx 0$ to $z \approx 2$; e.g., A. Merloni et al. 2010; B. Trakhtenbrot & H. Netzer 2010). As a basic estimate of the impact of such evolution, $\langle \lambda_{\text{Edd}} \rangle$

decreases by ≈ 0.3 dex and $\langle M_{\text{BH}} \rangle$ increases by ≈ 0.3 dex at $z = 2.0 - 2.5$, while the results at $z = 0.2 - 0.5$ remain unchanged in Figure 4. Thus, $\Delta \log \langle \lambda_{\text{Edd}} \rangle \approx -1.0$ dex and $\Delta \log \langle M_{\text{BH}} \rangle \approx -0.5$ dex from $z \approx 2$ to $z \approx 0.2$. This estimate does not alter our overall conclusion that the decline in $\langle \lambda_{\text{Edd}} \rangle$ is the primary driver of the broad decline in ρ_{BHAR} . It should also be noted that an evolving observed M_{BH}/M_* ratio does not necessarily imply evolution of the underlying $M_{\text{BH}} - M_*$ relation if selection bias is not properly taken into account. For example, in the $M_{\text{BH}} \propto M_*^{1.61}$ relation of J. E. Greene et al. (2020), selection bias may suppress the detection of lower-mass galaxies at higher redshift, leading to an apparently higher M_{BH}/M_* ratio ($M_{\text{BH}}/M_* \propto M_*^{0.61}$) even if the $M_{\text{BH}} - M_*$ relation itself does not evolve. In this case, our results would not differ significantly, as shown in Table 1.

One systematic bias arises from potentially missed CT accretion. However, as discussed in Section 2.1, this appears to affect ρ_{BHAR} by $\lesssim 0.2$ dex over the $z \lesssim 2$ range applicable to this paper. Another source of systematic uncertainty involves k_X . We tested the k_X from G. Yang et al. (2018) (a modification of E. Lusso et al. 2012) and found no material differences in the results. Additionally, while $\langle \lambda_{\text{Edd}} \rangle$ and $\langle M_{\text{BH}} \rangle$ lack universally

Table 1. $\log \rho_{\text{BHAR}}$, $\log \langle \lambda_{\text{Edd}} \rangle$, $\log \langle M_{\text{BH}} \rangle$, and $\log n_{\text{AGN}}^{\text{eff}}$ at different redshifts bins and their declines.

z	0.2 – 0.5	0.5 – 0.8	0.8 – 1.1	1.1 – 1.5	1.5 – 2.0	2.0 – 2.5	2.5 – 3.0	3.0 – 3.5	3.5 – 4.0	Δ (dex)
$\log \rho_{\text{BHAR}}$	$-5.83^{+0.07}_{-0.06}$	$-5.32^{+0.05}_{-0.05}$	$-4.83^{+0.05}_{-0.04}$	$-4.58^{+0.05}_{-0.04}$	$-4.54^{+0.05}_{-0.05}$	$-4.61^{+0.06}_{-0.07}$	$-4.86^{+0.08}_{-0.08}$	$-4.75^{+0.09}_{-0.09}$	$-5.33^{+0.17}_{-0.17}$	$-1.28^{+0.08}_{-0.08}$
$\log \langle \lambda_{\text{Edd}} \rangle$	$-1.59^{+0.27}_{-0.20}$	$-1.33^{+0.24}_{-0.20}$	$-0.90^{+0.30}_{-0.30}$	$-0.51^{+0.28}_{-0.27}$	$-0.24^{+0.34}_{-0.33}$	$-0.27^{+0.34}_{-0.32}$	$-0.16^{+0.40}_{-0.41}$	$0.20^{+0.34}_{-0.35}$	$0.35^{+0.63}_{-0.67}$	$-1.35^{+0.46}_{-0.39}$
$\log \langle M_{\text{BH}} \rangle$	$7.96^{+0.10}_{-0.05}$	$8.05^{+0.05}_{-0.05}$	$8.16^{+0.09}_{-0.05}$	$8.30^{+0.06}_{-0.09}$	$8.17^{+0.10}_{-0.06}$	$8.22^{+0.09}_{-0.07}$	$8.15^{+0.16}_{-0.14}$	$8.26^{+0.15}_{-0.10}$	$7.89^{+0.16}_{-0.15}$	$-0.21^{+0.11}_{-0.11}$
$\log n_{\text{AGN}}^{\text{eff}}$	$-4.50^{+0.21}_{-0.29}$	$-4.33^{+0.19}_{-0.20}$	$-4.40^{+0.23}_{-0.27}$	$-4.66^{+0.26}_{-0.29}$	$-4.78^{+0.32}_{-0.34}$	$-4.87^{+0.35}_{-0.38}$	$-5.13^{+0.46}_{-0.51}$	$-5.54^{+0.42}_{-0.34}$	$-5.88^{+0.71}_{-0.61}$	$0.29^{+0.38}_{-0.46}$
$\log \rho_{\text{BHAR}}$	$-5.81^{+0.06}_{-0.06}$	$-5.32^{+0.05}_{-0.05}$	$-4.84^{+0.04}_{-0.05}$	$-4.59^{+0.05}_{-0.05}$	$-4.56^{+0.05}_{-0.05}$	$-4.62^{+0.06}_{-0.06}$	$-4.88^{+0.08}_{-0.07}$	$-4.76^{+0.09}_{-0.08}$	$-5.36^{+0.16}_{-0.16}$	$-1.26^{+0.08}_{-0.08}$
$\log \langle \lambda_{\text{Edd}} \rangle$	$-1.45^{+0.29}_{-0.26}$	$-1.20^{+0.30}_{-0.23}$	$-0.83^{+0.37}_{-0.31}$	$-0.49^{+0.35}_{-0.26}$	$-0.16^{+0.45}_{-0.51}$	$-0.23^{+0.36}_{-0.34}$	$-0.04^{+0.57}_{-0.43}$	$0.27^{+0.40}_{-0.36}$	$0.59^{+0.70}_{-0.66}$	$-1.28^{+0.58}_{-0.53}$
$\log \langle M_{\text{BH}} \rangle$	$7.80^{+0.22}_{-0.19}$	$7.90^{+0.14}_{-0.13}$	$8.06^{+0.21}_{-0.11}$	$8.28^{+0.10}_{-0.17}$	$8.05^{+0.23}_{-0.10}$	$8.20^{+0.14}_{-0.10}$	$8.03^{+0.18}_{-0.25}$	$8.18^{+0.18}_{-0.15}$	$7.61^{+0.25}_{-0.24}$	$-0.25^{+0.26}_{-0.31}$
$\log n_{\text{AGN}}^{\text{eff}}$	$-4.49^{+0.16}_{-0.16}$	$-4.33^{+0.13}_{-0.16}$	$-4.38^{+0.16}_{-0.27}$	$-4.67^{+0.18}_{-0.31}$	$-4.76^{+0.34}_{-0.40}$	$-4.88^{+0.33}_{-0.37}$	$-5.17^{+0.40}_{-0.49}$	$-5.53^{+0.37}_{-0.35}$	$-5.89^{+0.73}_{-0.63}$	$0.27^{+0.44}_{-0.39}$
N_{X}	873	1198	1367	1570	1281	563	246	136	34	Total: 7268
N_{gal}	325578	360191	253990	186904	105648	40967	22843	12252	4919	Total: 1313292

NOTE—The first part of the table shows the results assuming $M_{\text{BH}} = 0.002 M_{\star}$, while the second part adopts the relation $\log M_{\text{BH}} = 7.43 + 1.61 \log(M_{\star}/M_0)$ with $M_0 = 3 \times 10^{10} M_{\odot}$ (J. E. Greene et al. 2020). The uncertainties represent the 90% confidence intervals derived from 1000 Monte Carlo trials. “ Δ ” indicates the difference between the $z = 0.2 - 0.5$ and $z = 1.5 - 2.0$ bins, with negative values indicating a decline toward lower redshifts. The last two rows show the number of X-ray AGNs (N_{X}) and the number of normal galaxies (N_{gal}) above the M_{\star} -completeness limits.

precise definitions, their determination is supported by the consistency between $n_{\text{AGN}}^{\text{eff}}$ and n_{AGN} for AGNs with $\langle \lambda_{\text{Edd}} \rangle$ in Figure 5, indicating that our methodology is robust.

Although our results robustly reveal the primary cause for the decline in SMBH growth at $z \lesssim 2$ thanks to the well-constrained $p(\lambda_{\text{Edd}}|M_{\star}, z)$, we do not attempt to explain the rise in SMBH growth from $z \approx 4$ to $z \approx 2$ with the same methodology. This is mainly because of the higher obscured AGN fraction at $z > 2$ and the emerging evidence that there may be more hidden accretion power than previously expected. It is found that the obscured AGN fraction in X-rays appears to increase with redshift (e.g., J. Buchner et al. 2015; T. Liu et al. 2017; F. Vito et al. 2018; J. Lyu et al. 2024). Also, new JWST results indicate that some AGNs may be missed by X-ray surveys, even after accounting for observational biases. For example, many apparent X-ray weak AGNs were discovered by JWST at $z \gtrsim 2$ (e.g., D. D. Kocevski et al. 2025; R. Maiolino et al. 2025). These AGNs may be heavily obscured in X-rays or intrinsically X-ray weak. G. Yang et al. (2021) showed that the X-ray-inferred ρ_{BHAR} may be underestimated by a factor of a few at $z > 3$. Such a discrepancy mainly occurs at high redshift and does not have a significant impact on our analyses of the decline at $z \lesssim 2$. It is worthwhile to explore the cause of this discrepancy and quantify the impact of the higher M_{BH}/M_{\star} ratio observed among JWST-selected X-ray-weak AGNs (e.g., D. D. Kocevski et al. 2025) on ρ_{BHAR} at $z > 3$, but such efforts are beyond the scope of this paper.

3.2. Does M_{\star} Mainly Modulate the Typical Outburst Luminosity or Duty Cycle to Reduce SMBH Growth?

In this subsection, we investigate the decline in $\overline{\text{BHAR}}$ as M_{\star} decreases at fixed redshift, as per key question 2. With a similar approach to that in Section 3.1, $\overline{\text{BHAR}}$ can be approximately factored into two components and a constant factor at fixed (M_{\star}, z) :

$$\overline{\text{BHAR}} = \overline{L_{\text{bol}}^{\text{AGN}}} \times f_{\text{AGN}} \times \frac{(1 - \epsilon) \kappa(M_{\star})}{\epsilon c^2}, \quad (14)$$

where $\overline{L_{\text{bol}}^{\text{AGN}}}$ is the sample-averaged outburst luminosity per AGN and f_{AGN} is the AGN duty cycle (or equivalently the AGN fraction). Note that our $\overline{\text{BHAR}}$ is based upon the sample-averaged L_{bol} per galaxy, which is different from $\overline{L_{\text{bol}}^{\text{AGN}}}$. M_{\star} can modulate $\overline{L_{\text{bol}}^{\text{AGN}}}$ or f_{AGN} to change $\overline{\text{BHAR}}$.

We can calculate the f_{AGN} for galaxies if we regard SMBHs in those galaxies accreting above a given λ_{Edd} ($\lambda_{\text{Edd}}^{\text{min}}$) as AGNs:

$$f_{\text{AGN}} = \int_{\log \lambda_{\text{Edd}}^{\text{min}}}^{+\infty} p(\lambda_{\text{Edd}}|M_{\star}, z) d \log \lambda_{\text{Edd}}. \quad (15)$$

On the other hand, the $\overline{L_{\text{bol}}^{\text{AGN}}}$ can be calculated as

$$\begin{aligned} \overline{L_{\text{bol}}^{\text{AGN}}} = \int_{\log \lambda_{\text{Edd}}^{\text{min}}}^{+\infty} M_{\star} \lambda_{\text{Edd}} \kappa(M_{\star}) \\ \times p(\lambda_{\text{Edd}}|M_{\star}, z) / f_{\text{AGN}} d \log \lambda_{\text{Edd}}. \end{aligned} \quad (16)$$

The term $p(\lambda_{\text{Edd}}|M_{\star}, z)/f_{\text{AGN}}$ represents the conditional probability that an AGN with M_{\star} and z accretes

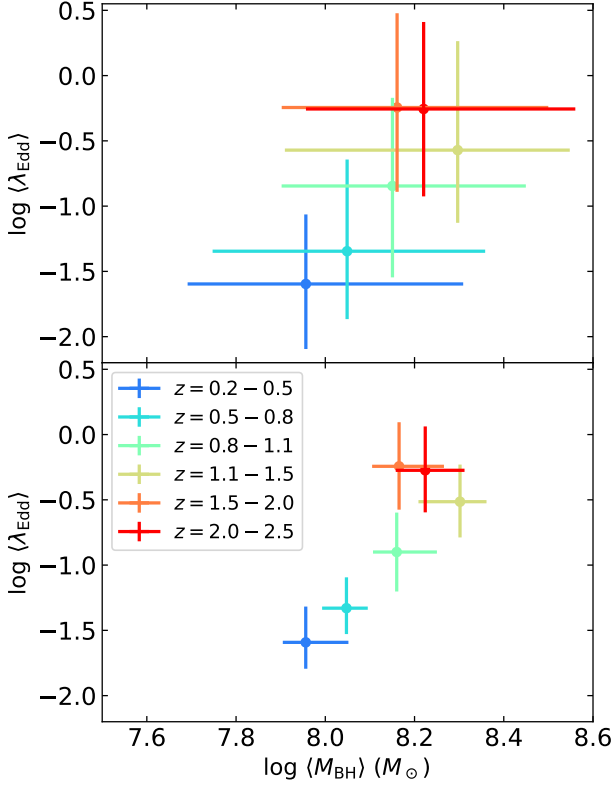


Figure 4. The evolution of $\langle\lambda_{\text{Edd}}\rangle$ and $\langle M_{\text{BH}}\rangle$ at different redshifts, with colors defined in the legend. Top panel: The error bars show the region bounded by the 25 – 75% quantiles of $\log \lambda_{\text{Edd}}$ and $\log \langle M_{\text{BH}}\rangle$ in Figure 3 assuming the median $p(\lambda_{\text{Edd}}|M_*, z)$ and $M_{\text{BH}} = 0.002M_*$. Bottom panel: The error bars represent the 90% confidence intervals derived with our Monte Carlo method. From $z = 1.5 - 2.0$ to $z = 0.2 - 0.5$, $\langle\lambda_{\text{Edd}}\rangle$ and $\langle M_{\text{BH}}\rangle$ both decrease; $\langle\lambda_{\text{Edd}}\rangle$ decreases by 1.35 dex, but $\langle M_{\text{BH}}\rangle$ decreases only by 0.21 dex.

at λ_{Edd} . We set $\lambda_{\text{Edd}}^{\min} = 0.01$ following J. Aird et al. (2018).

The top panels of Figure 6 show $\overline{L_{\text{bol}}^{\text{AGN}}}$ and f_{AGN} as functions of redshift at different M_* . M_* strongly modulates $\overline{L_{\text{bol}}^{\text{AGN}}}$ at all redshifts. This behavior generally reflects the $M_{\text{BH}} - M_*$ relation, where more massive galaxies host more massive SMBHs. Without a strict dependence of λ_{Edd} on M_* at fixed redshift, more massive galaxies tend to host more luminous AGNs. $\overline{L_{\text{bol}}^{\text{AGN}}}$ also slightly decreases toward lower redshift at fixed M_* . With our assumption of a linear scaling between M_{BH} and M_* , this result indicates a slight decrease in λ_{Edd} . The small decrease in λ_{Edd} here does not contradict the large evolution of $\langle\lambda_{\text{Edd}}\rangle$ in Section 3.1.2, because $\langle\lambda_{\text{Edd}}\rangle$ characterizes the typical λ_{Edd} for the AGNs contributing most of ρ_{BHAR} , while $\overline{L_{\text{bol}}^{\text{AGN}}}$ is simply the average L_{bol} of AGNs. n_{AGN} is dominated by low- λ_{Edd} AGNs at all redshifts as shown in Figure 5, causing a less-

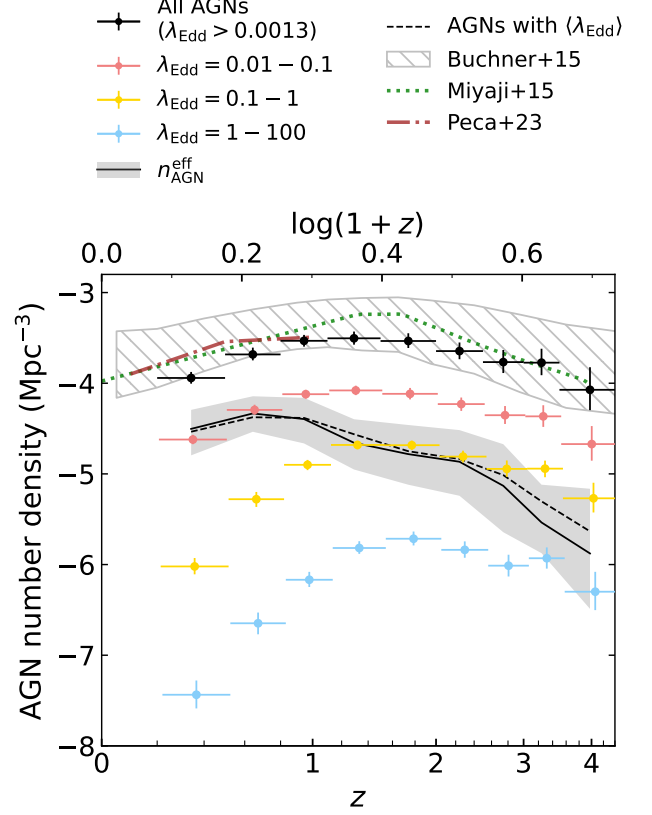


Figure 5. n_{AGN} and $n_{\text{AGN}}^{\text{eff}}$ as a function of redshift. The black data points represent the total n_{AGN} sampled by our data ($\lambda_{\text{Edd}} > 0.0013$). The red, yellow, and blue data points represent n_{AGN} for AGNs accreting at $\lambda_{\text{Edd}} = 0.01 - 0.1$, $\lambda_{\text{Edd}} = 0.1 - 1$, and $\lambda_{\text{Edd}} = 1 - 100$, respectively. The black solid line represents $n_{\text{AGN}}^{\text{eff}}$, and the dashed line represents n_{AGN} for AGNs within the 25–75% quantile range of $\langle\lambda_{\text{Edd}}\rangle$. The error bars of the data points and the grey shaded region for $n_{\text{AGN}}^{\text{eff}}$ represent the 90% confidence intervals derived with our Monte Carlo method. For comparison, we show the total n_{AGN} for AGNs with $\log L_X > 42$ from J. Buchner et al. (2015) (grey hatched region representing 10–90% confidence intervals), T. Miyaji et al. (2015) (green dotted line), and A. Peca et al. (2023) (brown dotted-dashed line).

significant evolution of the average λ_{Edd} . On the other hand, in Figure 6 top-right panel, f_{AGN} is almost independent of M_* at low redshift and is clearly dependent on M_* only at $z \gtrsim 1$. At fixed M_* , f_{AGN} show stronger redshift evolution in more massive galaxies. Such behavior for f_{AGN} has been found in previous works (e.g., J. Aird et al. 2018, 2019; K. L. Birchall et al. 2022). At $z \gtrsim 1$, larger amounts of gas are available (e.g., R. Decarli et al. 2019), which tends to trigger luminous AGNs in massive galaxies with massive SMBHs and deeper potential wells (e.g., Y. M. Rosas-Guevara et al. 2015). As redshift decreases, the lack of available gas starves lumi-

nous AGNs, causing a more significant decline in f_{AGN} in massive galaxies.

The bottom panel of Figure 6 shows the declines in $\overline{\text{BHAR}}$, $\overline{L_{\text{bol}}^{\text{AGN}}}$, and f_{AGN} from $\log M_{\star} = 11.5$ to $\log M_{\star} = 10$ as functions of redshift. These two $\log M_{\star}$ values are chosen for illustration because our measurements at these masses are well-constrained. At $z \lesssim 1$, the decline in $\overline{\text{BHAR}}$ is driven almost entirely by $\overline{L_{\text{bol}}^{\text{AGN}}}$. At $z \gtrsim 1$, the decline in f_{AGN} is only about 0.3–0.7 dex, which is more than 10 times smaller than the decline in $\overline{L_{\text{bol}}^{\text{AGN}}}$ (1.4–2.0 dex).

Overall, our results indicate that M_{\star} predominantly regulates $\overline{L_{\text{bol}}^{\text{AGN}}}$ instead of f_{AGN} to drive variations in $\overline{\text{BHAR}}$. These results are also generally consistent with those from J. Aird et al. (2018) in their Figures 6 and 8, where higher- M_{\star} galaxies exhibit a higher f_{AGN} than lower- M_{\star} galaxies at $z \gtrsim 1$, and the decrease in $\overline{L_{\text{bol}}^{\text{AGN}}}$ for lower- M_{\star} galaxies is slightly faster than that for higher- M_{\star} galaxies. Our measurements provide superior constraints for a wide M_{\star} range than those from J. Aird et al. (2018) thanks to the larger survey volume of XMM-SERVS and eFEDS. We also test the nonlinear $M_{\text{BH}} - M_{\star}$ relation of J. E. Greene et al. (2020) in our analyses and find an even higher fractional contribution of $\overline{L_{\text{bol}}^{\text{AGN}}}$ to the variation in $\overline{\text{BHAR}}$. This arises because the nonlinear relation ($M_{\text{BH}} \propto M_{\star}^{1.61}$) imposes a stronger M_{\star} -dependence than the linear case, yielding larger differences in M_{BH} between galaxies of different M_{\star} , and thus enhancing the contribution of $\overline{L_{\text{bol}}^{\text{AGN}}}$ in driving the variation in $\overline{\text{BHAR}}$.

4. SUMMARY AND FUTURE WORK

In this work, we leverage the best-measured sample-averaged SMBH accretion rates in F. Zou et al. (2024) to understand and quantify the decline in SMBH growth at $z \lesssim 2$. Our main results are summarized as follows:

1. We confirm that ρ_{BHAR} peaks at $z \approx 2$ and declines dramatically since then. We find that low-accretion activity gradually dominates the contribution to ρ_{BHAR} as redshift decreases. At $z \gtrsim 1$, ρ_{BHAR} is mostly contributed by rapidly accreting SMBHs, while at $z \lesssim 0.5$, $\lambda_{\text{Edd}} < 0.1$ activity dominates ρ_{BHAR} . See Section 3.1.1.
2. From $z \approx 2$ to $z \approx 0.2$, the decline in ρ_{BHAR} is mainly driven by the decline in λ_{Edd} ($\Delta \log \langle \lambda_{\text{Edd}} \rangle = -1.35_{-0.39}^{+0.46}$ dex) rather than M_{BH} ($\Delta \log \langle M_{\text{BH}} \rangle = -0.21_{-0.11}^{+0.11}$ dex). On the other hand, $n_{\text{AGN}}^{\text{eff}}$ is generally constant (increasing by $0.29_{-0.46}^{+0.38}$ dex) due to the significantly lower $\langle \lambda_{\text{Edd}} \rangle$ at lower redshift, the decreasing total n_{AGN} , and the fact that the low- λ_{Edd} AGN number density

dominates the total n_{AGN} at all redshifts. See Section 3.1.2.

3. The observed dependence of $\overline{\text{BHAR}}$ on M_{\star} at fixed redshift arises primarily because M_{\star} predominantly regulates $\overline{L_{\text{bol}}^{\text{AGN}}}$ instead of f_{AGN} to drive variations in $\overline{\text{BHAR}}$. f_{AGN} shows stronger redshift evolution in more massive galaxies, which may be due to the availability of cold gas preferentially affecting luminous AGNs in massive galaxies. See Section 3.2.

Overall, our results clarify the primary cause of the decline in SMBH growth at $z < 2$ and provide new insight into the AGN downsizing phenomenon. Previous studies suggest that AGN downsizing does not reflect antihierarchical behavior, but instead results from a combination of factors, e.g., λ_{Edd} and M_{BH} , where λ_{Edd} may play a more important role (e.g., A. Babić et al. 2007; N. Fanidakis et al. 2012; J. Aird et al. 2015; H. Suh et al. 2015). Our findings provide the most compelling evidence to date that λ_{Edd} plays the primary role in driving AGN downsizing.

There are several ways to extend this work with better datasets in the future. For example, there are existing wide-field X-ray surveys by Chandra and/or XMM-Newton with generally sufficient quality multi-wavelength coverage, such as the Chandra Deep Wide-Field Survey (CDWFS; e.g., A. Masini et al. 2020), XMM-XXL (e.g., M. Pierre et al. 2016), Stripe 82X (e.g., S. M. LaMassa et al. 2016), and Stripe 82-XL (e.g., A. Peca et al. 2024), totaling $\sim 100 \text{ deg}^2$. Future work could include these surveys in the “wedding-cake” design to help sample AGNs at low redshift and/or high luminosity. There are also other very wide-field X-ray catalogs above 2 keV—such as the Chandra Source Catalog (e.g., I. N. Evans et al. 2024), 4XMM (e.g., N. A. Webb et al. 2020), and the Swift/BAT catalog (e.g., A. Y. Lien et al. 2025)—providing a much larger survey volume with reduced obscuration effects, particularly valuable for sampling the most luminous AGNs. Soon, these catalogs will benefit from excellent multi-wavelength coverage provided by new photometric and spectroscopic surveys such as LSST (e.g., Ž. Ivezić et al. 2019), Euclid (e.g., Euclid Collaboration et al. 2024), Roman (e.g., R. Akeson et al. 2019), Wide Field Survey Telescope (WFST; e.g., T. Wang et al. 2023), Chinese Space Station Survey Telescope (CSST; e.g., CSST Collaboration et al. 2025), SPHEREx (e.g., B. P. Crill et al. 2020), 4m Multi-Object Spectroscopic Telescope (4MOST; e.g., R. S. de Jong et al. 2019), Subaru Prime Focus Spectrograph (PFS; e.g., M. Takada et al. 2014), and Dark Energy Spectroscopic Instrument (DESI; e.g.,

Table 2. Smoothed double power-law fits to the redshift evolution of ρ_{BHAR} and n_{AGN} .

	ρ_{BHAR}				n_{AGN}			
	All AGNs	$\lambda_{\text{Edd}} = 0.01 - 0.1$	$\lambda_{\text{Edd}} = 0.1 - 1$	$\lambda_{\text{Edd}} = 1 - 100$	All AGNs	$\lambda_{\text{Edd}} = 0.01 - 0.1$	$\lambda_{\text{Edd}} = 0.1 - 1$	$\lambda_{\text{Edd}} = 1 - 100$
$\log A$	-4.20 ± 0.09	-4.93 ± 0.07	-4.64 ± 0.09	-4.59 ± 0.11	-3.20 ± 0.03	-3.78 ± 0.04	-4.42 ± 0.06	-5.49 ± 0.07
z_0	1.48 ± 0.21	1.31 ± 0.20	1.39 ± 0.15	1.48 ± 0.18	1.18 ± 0.22	1.12 ± 0.18	1.13 ± 0.09	1.29 ± 0.11
γ_1	3.30 ± 0.83	3.56 ± 0.68	3.39 ± 0.73	2.85 ± 0.85	2.29 ± 0.40	2.24 ± 0.36	2.09 ± 0.33	2.16 ± 0.45
γ_2	-6.07 ± 0.99	-5.15 ± 1.07	-7.77 ± 1.02	-7.86 ± 1.03	-3.36 ± 0.73	-4.07 ± 0.75	-7.84 ± 0.74	-8.23 ± 0.74

NOTE—The second through fifth columns and the last four columns show the best-fit results for ρ_{BHAR} and n_{AGN} , respectively. The uncertainties represent 1σ confidence intervals.

DESI Collaboration et al. 2025). These complementary datasets will allow the construction of massive samples of well-characterized X-ray AGNs with robust redshifts and host-galaxy properties. Also, future deep X-ray surveys by the NewAthena (e.g., M. Cruise et al. 2025), AXIS (e.g., C. S. Reynolds et al. 2023), and Lynx (e.g., J. A. Gaskin et al. 2019) missions can probe AGN populations with higher obscuration, which can constrain the missed population caused by obscuration.

ACKNOWLEDGMENTS

We thank the anonymous referee for constructive feedback. ZY and WNB acknowledge support from NSF grants AST-2106990 and AST-2407089 and Chandra X-ray Center grant AR4-25008X. FV acknowledges support from “INAF Ricerca Fondamentale 2023 - Large GO” grant.

APPENDIX

A. RESULTS WITHOUT EFEDS

eFEDS is mainly observed in soft X-rays below 2.3 keV, which makes it more easily affected by obscuration (though, as discussed in Section 2.1, corrections have been made for obscured accretion power). In this Appendix, we test if eFEDS introduces significant bias by excluding eFEDS from our analyses, and our main results in Section 3.1 are shown in Figure 7. After excluding eFEDS, the results for ρ_{BHAR} and n_{AGN} in different λ_{Edd} bins generally exhibit larger uncertainties at $z \lesssim 1$, but their median values remain consistent with those including eFEDS within the 90% confidence intervals. These results demonstrate that eFEDS does not lead to significant bias, nor does excluding eFEDS alter the overall conclusion that the broad decline in ρ_{BHAR} is mainly driven by the decline in $\langle \lambda_{\text{Edd}} \rangle$. In addition to the other fields covering $\approx 13 \text{ deg}^2$ that are observed from $\approx 2 - 10 \text{ keV}$, the 60 deg^2 eFEDS field provides useful constraints at $z \lesssim 1$ by increasing the number of X-ray AGNs at $z \lesssim 1$ by $\approx 60\%$, thereby allowing more accurate measurements of the SMBH growth decline at $z \lesssim 2$.

B. FUNCTIONAL FITS TO THE REDSHIFT EVOLUTION OF ρ_{BHAR} AND n_{AGN}

In Section 3.1, we show that ρ_{BHAR} and n_{AGN} in different redshift and λ_{Edd} bins can be calculated using Equations 9 and 12, respectively. In this Appendix, we present simple functional fits to their redshift evolution at $z < 4$ using a smoothed double power-law:

$$\rho_{\text{BHAR}}(z) \text{ or } n_{\text{AGN}}(z) = A \left[\left(\frac{1+z}{1+z_0} \right)^{\gamma_1} + \left(\frac{1+z}{1+z_0} \right)^{\gamma_2} \right]^{-1}, \quad (\text{B1})$$

where A is the normalization, z_0 is approximately the redshift where ρ_{BHAR} or n_{AGN} peaks, and γ_1 and γ_2 are the different slopes before and after z_0 , as seen in our Figures 1 and 5. Such a functional form is similar to the broken power-law shape of the redshift evolution term adopted in the luminosity-dependent density evolution (LDDE) model (e.g., Y. Ueda et al. 2014; J. Aird et al. 2015; J. Buchner et al. 2015; E. Pouliasis et al. 2024). However, we do not consider any λ_{Edd} or L_X dependence, and we fit ρ_{BHAR} and n_{AGN} in different λ_{Edd} bins separately. We use a least-squares method to fit our median data points assuming the linear $M_{\text{BH}} - M_\star$ relation, and the best-fit parameters are summarized in Table 2.

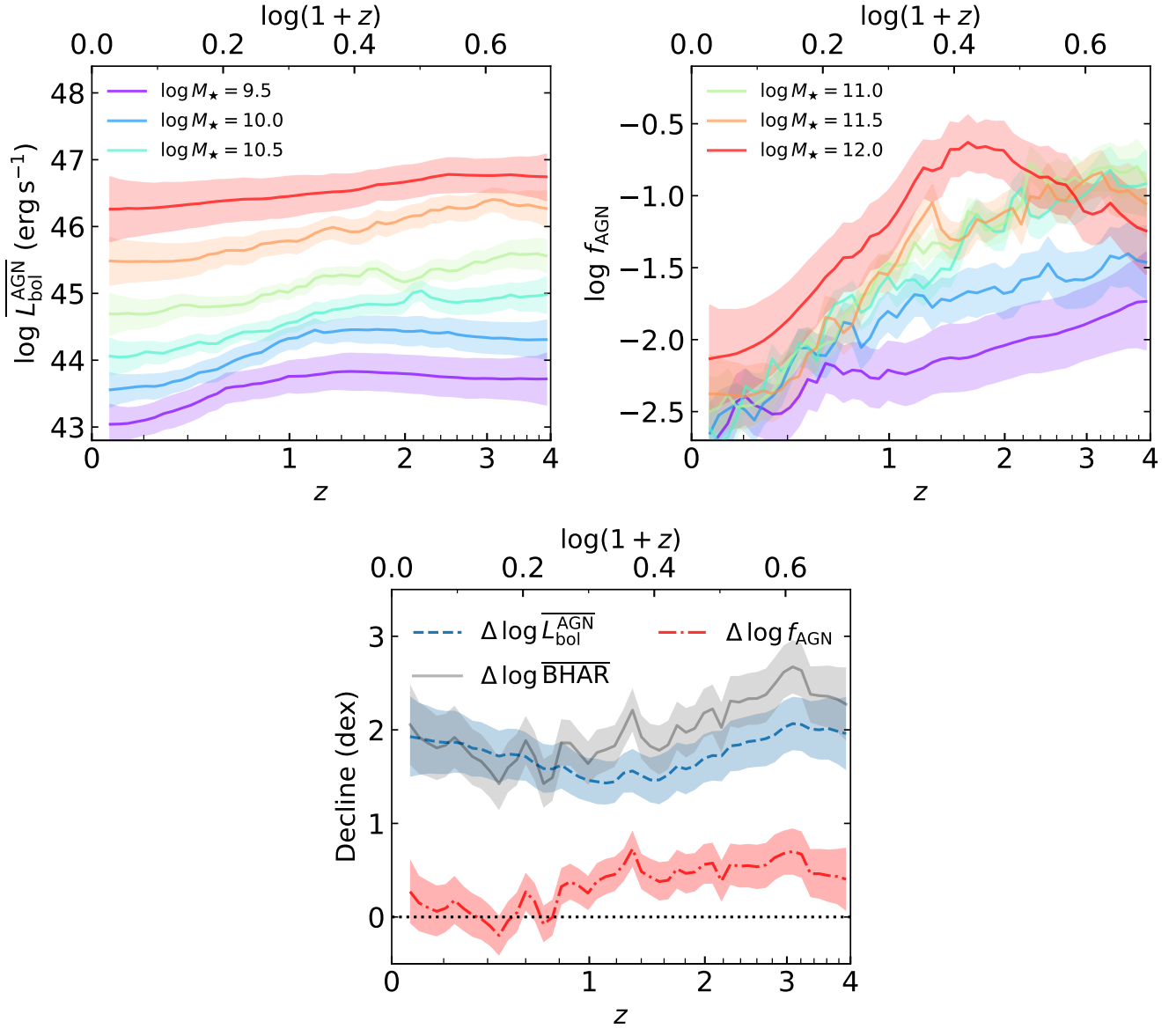


Figure 6. Top panels: $\overline{L}_{\text{bol}}^{\text{AGN}}$ (top-left) and f_{AGN} (top-right) as functions of redshift at different M_{\star} , with colors defined in the legend. Bottom panel: The decline in $\overline{\text{BHAR}}$ (grey solid), $\overline{L}_{\text{bol}}^{\text{AGN}}$ (blue dashed), and f_{AGN} (red dash-dotted) from $\log M_{\star} = 11.5$ to $\log M_{\star} = 10$ as functions of redshift. The colored shaded stripes represent the 1 σ uncertainty from $p(\lambda_{\text{Edd}}|M_{\star}, z)$.

REFERENCES

- Aird, J., Coil, A. L., & Georgakakis, A. 2018, MNRAS, 474, 1225, doi: [10.1093/mnras/stx2700](https://doi.org/10.1093/mnras/stx2700)
- Aird, J., Coil, A. L., & Georgakakis, A. 2019, MNRAS, 484, 4360, doi: [10.1093/mnras/stz125](https://doi.org/10.1093/mnras/stz125)
- Aird, J., Coil, A. L., Georgakakis, A., et al. 2015, MNRAS, 451, 1892, doi: [10.1093/mnras/stv1062](https://doi.org/10.1093/mnras/stv1062)
- Aird, J., Coil, A. L., Moustakas, J., et al. 2012, ApJ, 746, 90, doi: [10.1088/0004-637X/746/1/90](https://doi.org/10.1088/0004-637X/746/1/90)
- Akeson, R., Armus, L., Bachelet, E., et al. 2019, arXiv e-prints, arXiv:1902.05569, doi: [10.48550/arXiv.1902.05569](https://doi.org/10.48550/arXiv.1902.05569)
- Alexander, D. M., Hickox, R. C., Aird, J., et al. 2025, NewAR, 101, 101733, doi: [10.1016/j.newar.2025.101733](https://doi.org/10.1016/j.newar.2025.101733)
- Ananna, T. T., Treister, E., Urry, C. M., et al. 2019, ApJ, 871, 240, doi: [10.3847/1538-4357/aafb77](https://doi.org/10.3847/1538-4357/aafb77)
- Babić, A., Miller, L., Jarvis, M. J., et al. 2007, A&A, 474, 755, doi: [10.1051/0004-6361:20078286](https://doi.org/10.1051/0004-6361:20078286)

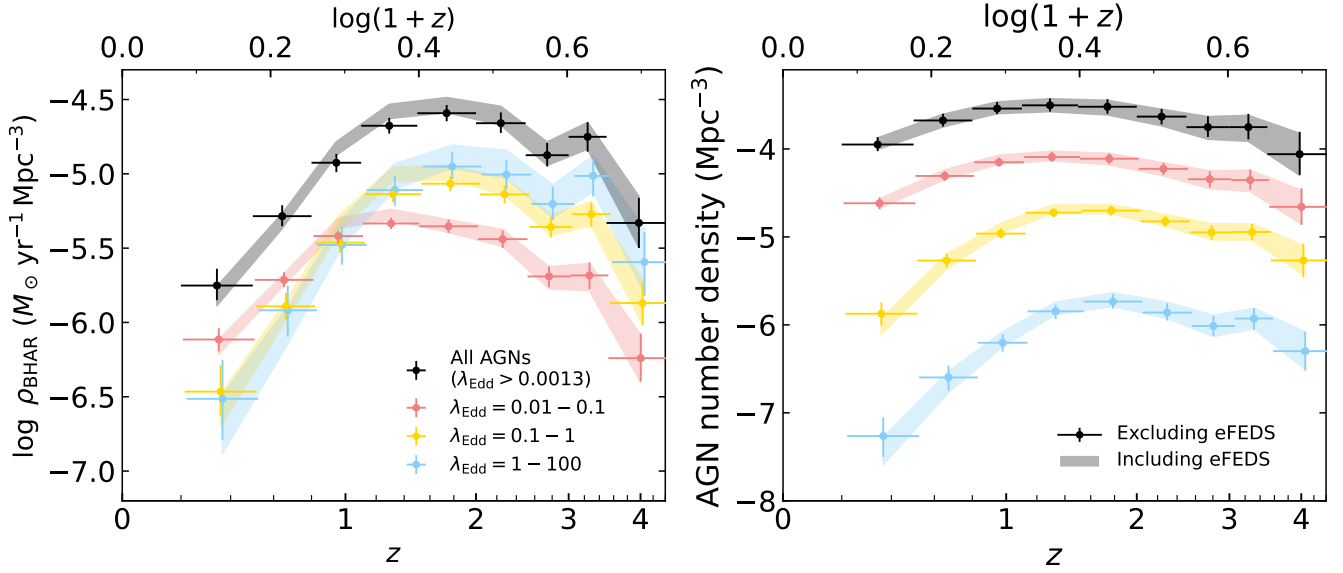


Figure 7. Comparison of ρ_{BHAR} (left panel) and n_{AGN} (right panel) for results excluding eFEDS (data points with error bars) and including eFEDS (shaded regions). Error bars and shaded regions indicate 90% statistical uncertainties, with colors matching those in the legend of the left panel.

Barger, A. J., Cowie, L. L., Mushotzky, R. F., et al. 2005, *AJ*, 129, 578, doi: [10.1086/426915](https://doi.org/10.1086/426915)

Barlow-Hall, C. L., & Aird, J. 2025, arXiv e-prints, arXiv:2506.16145, doi: [10.48550/arXiv.2506.16145](https://doi.org/10.48550/arXiv.2506.16145)

Birchall, K. L., Watson, M. G., Aird, J., & Starling, R. L. C. 2022, *MNRAS*, 510, 4556, doi: [10.1093/mnras/stab3573](https://doi.org/10.1093/mnras/stab3573)

Bongiorno, A., Merloni, A., Brusa, M., et al. 2012, *MNRAS*, 427, 3103, doi: [10.1111/j.1365-2966.2012.22089.x](https://doi.org/10.1111/j.1365-2966.2012.22089.x)

Brandt, W. N., & Alexander, D. M. 2015, *A&A Rv*, 23, 1, doi: [10.1007/s00159-014-0081-z](https://doi.org/10.1007/s00159-014-0081-z)

Brandt, W. N., & Yang, G. 2022, in *Handbook of X-ray and Gamma-ray Astrophysics*, 78, doi: [10.1007/978-981-16-4544-0_130-1](https://doi.org/10.1007/978-981-16-4544-0_130-1)

Brandt, W. N., Ni, Q., Yang, G., et al. 2018, arXiv e-prints, arXiv:1811.06542, doi: [10.48550/arXiv.1811.06542](https://doi.org/10.48550/arXiv.1811.06542)

Buchner, J., Georgakakis, A., Nandra, K., et al. 2015, *ApJ*, 802, 89, doi: [10.1088/0004-637X/802/2/89](https://doi.org/10.1088/0004-637X/802/2/89)

Chen, C.-T. J., Brandt, W. N., Luo, B., et al. 2018, *MNRAS*, 478, 2132, doi: [10.1093/mnras/sty1036](https://doi.org/10.1093/mnras/sty1036)

Civano, F., Marchesi, S., Comastri, A., et al. 2016, *ApJ*, 819, 62, doi: [10.3847/0004-637X/819/1/62](https://doi.org/10.3847/0004-637X/819/1/62)

Cowie, L. L., Barger, A. J., Bautz, M. W., Brandt, W. N., & Garmire, G. P. 2003, *ApJL*, 584, L57, doi: [10.1086/368404](https://doi.org/10.1086/368404)

Crill, B. P., Werner, M., Akeson, R., et al. 2020, in *Society of Photo-Optical Instrumentation Engineers (SPIE) Conference Series*, Vol. 11443, *Space Telescopes and Instrumentation 2020: Optical, Infrared, and Millimeter Wave*, ed. M. Lystrup & M. D. Perrin, 114430I, doi: [10.1117/12.2567224](https://doi.org/10.1117/12.2567224)

Cruise, M., Guainazzi, M., Aird, J., et al. 2025, *Nature Astronomy*, 9, 36, doi: [10.1038/s41550-024-02416-3](https://doi.org/10.1038/s41550-024-02416-3)

CSST Collaboration, Gong, Y., Miao, H., et al. 2025, arXiv e-prints, arXiv:2507.04618, doi: [10.48550/arXiv.2507.04618](https://doi.org/10.48550/arXiv.2507.04618)

de Jong, R. S., Agertz, O., Berbel, A. A., et al. 2019, *The Messenger*, 175, 3, doi: [10.18727/0722-6691/5117](https://doi.org/10.18727/0722-6691/5117)

Decarli, R., Dotti, M., Bañados, E., et al. 2019, *ApJ*, 880, 157, doi: [10.3847/1538-4357/ab297f](https://doi.org/10.3847/1538-4357/ab297f)

Delvecchio, I., Daddi, E., Aird, J., et al. 2020, *ApJ*, 892, 17, doi: [10.3847/1538-4357/ab789c](https://doi.org/10.3847/1538-4357/ab789c)

DESI Collaboration, Abdul-Karim, M., Adame, A. G., et al. 2025, arXiv e-prints, arXiv:2503.14745, doi: [10.48550/arXiv.2503.14745](https://doi.org/10.48550/arXiv.2503.14745)

Di Matteo, T., Springel, V., & Hernquist, L. 2005, *Nature*, 433, 604, doi: [10.1038/nature03335](https://doi.org/10.1038/nature03335)

Duras, F., Bongiorno, A., Ricci, F., et al. 2020, *A&A*, 636, A73, doi: [10.1051/0004-6361/201936817](https://doi.org/10.1051/0004-6361/201936817)

Euclid Collaboration, Mellier, Y., Abdurro'uf, et al. 2024, arXiv e-prints, arXiv:2405.13491, doi: [10.48550/arXiv.2405.13491](https://doi.org/10.48550/arXiv.2405.13491)

Evans, I. N., Evans, J. D., Martínez-Galarza, J. R., et al. 2024, *ApJS*, 274, 22, doi: [10.3847/1538-4365/ad6319](https://doi.org/10.3847/1538-4365/ad6319)

- Fanidakis, N., Baugh, C. M., Benson, A. J., et al. 2012, *MNRAS*, 419, 2797, doi: [10.1111/j.1365-2966.2011.19931.x](https://doi.org/10.1111/j.1365-2966.2011.19931.x)
- Gallo, E., & Sesana, A. 2019, *ApJL*, 883, L18, doi: [10.3847/2041-8213/ab40c6](https://doi.org/10.3847/2041-8213/ab40c6)
- Gaskin, J. A., Swartz, D. A., Vikhlinin, A., et al. 2019, *Journal of Astronomical Telescopes, Instruments, and Systems*, 5, 021001, doi: [10.1117/1.JATIS.5.2.021001](https://doi.org/10.1117/1.JATIS.5.2.021001)
- Greene, J. E., Strader, J., & Ho, L. C. 2020, *ARA&A*, 58, 257, doi: [10.1146/annurev-astro-032620-021835](https://doi.org/10.1146/annurev-astro-032620-021835)
- Grogin, N. A., Kocevski, D. D., Faber, S. M., et al. 2011, *ApJS*, 197, 35, doi: [10.1088/0067-0049/197/2/35](https://doi.org/10.1088/0067-0049/197/2/35)
- Hasinger, G., Miyaji, T., & Schmidt, M. 2005, *A&A*, 441, 417, doi: [10.1051/0004-6361:20042134](https://doi.org/10.1051/0004-6361:20042134)
- Heckman, T. M., & Best, P. N. 2014, *ARA&A*, 52, 589, doi: [10.1146/annurev-astro-081913-035722](https://doi.org/10.1146/annurev-astro-081913-035722)
- Heckman, T. M., Kauffmann, G., Brinchmann, J., et al. 2004, *ApJ*, 613, 109, doi: [10.1086/422872](https://doi.org/10.1086/422872)
- Hopkins, P. F., & Hernquist, L. 2006, *ApJS*, 166, 1, doi: [10.1086/505753](https://doi.org/10.1086/505753)
- Hopkins, P. F., & Quataert, E. 2010, *MNRAS*, 407, 1529, doi: [10.1111/j.1365-2966.2010.17064.x](https://doi.org/10.1111/j.1365-2966.2010.17064.x)
- Hopkins, P. F., Richards, G. T., & Hernquist, L. 2007, *ApJ*, 654, 731, doi: [10.1086/509629](https://doi.org/10.1086/509629)
- Ivezić, Ž., Kahn, S. M., Tyson, J. A., et al. 2019, *ApJ*, 873, 111, doi: [10.3847/1538-4357/ab042c](https://doi.org/10.3847/1538-4357/ab042c)
- Kelly, B. C., & Shen, Y. 2013, *ApJ*, 764, 45, doi: [10.1088/0004-637X/764/1/45](https://doi.org/10.1088/0004-637X/764/1/45)
- Kocevski, D. D., Hasinger, G., Brightman, M., et al. 2018, *ApJS*, 236, 48, doi: [10.3847/1538-4365/aab9b4](https://doi.org/10.3847/1538-4365/aab9b4)
- Kocevski, D. D., Finkelstein, S. L., Barro, G., et al. 2025, *ApJ*, 986, 126, doi: [10.3847/1538-4357/adbc7d](https://doi.org/10.3847/1538-4357/adbc7d)
- Koekemoer, A. M., Faber, S. M., Ferguson, H. C., et al. 2011, *ApJS*, 197, 36, doi: [10.1088/0067-0049/197/2/36](https://doi.org/10.1088/0067-0049/197/2/36)
- Kormendy, J., & Ho, L. C. 2013, *ARA&A*, 51, 511, doi: [10.1146/annurev-astro-082708-101811](https://doi.org/10.1146/annurev-astro-082708-101811)
- LaMassa, S. M., Urry, C. M., Cappelluti, N., et al. 2016, *ApJ*, 817, 172, doi: [10.3847/0004-637X/817/2/172](https://doi.org/10.3847/0004-637X/817/2/172)
- Li, J., Xue, Y., Sun, M., et al. 2020, *ApJ*, 903, 49, doi: [10.3847/1538-4357/abb6e7](https://doi.org/10.3847/1538-4357/abb6e7)
- Li, J. I. H., Shen, Y., Ho, L. C., et al. 2023, *ApJ*, 954, 173, doi: [10.3847/1538-4357/acddda](https://doi.org/10.3847/1538-4357/acddda)
- Lien, A. Y., Krimm, H. A., Markwardt, C. B., et al. 2025, *ApJ*, 989, 161, doi: [10.3847/1538-4357/ade676](https://doi.org/10.3847/1538-4357/ade676)
- Liu, T., Tozzi, P., Wang, J.-X., et al. 2017, *ApJS*, 232, 8, doi: [10.3847/1538-4365/aa7847](https://doi.org/10.3847/1538-4365/aa7847)
- Liu, T., Buchner, J., Nandra, K., et al. 2022, *A&A*, 661, A5, doi: [10.1051/0004-6361/202141643](https://doi.org/10.1051/0004-6361/202141643)
- Luo, B., Brandt, W. N., Xue, Y. Q., et al. 2017, *ApJS*, 228, 2, doi: [10.3847/1538-4365/228/1/2](https://doi.org/10.3847/1538-4365/228/1/2)
- Lusso, E., Comastri, A., Simmons, B. D., et al. 2012, *MNRAS*, 425, 623, doi: [10.1111/j.1365-2966.2012.21513.x](https://doi.org/10.1111/j.1365-2966.2012.21513.x)
- Lyu, J., Alberts, S., Rieke, G. H., et al. 2024, *ApJ*, 966, 229, doi: [10.3847/1538-4357/ad3643](https://doi.org/10.3847/1538-4357/ad3643)
- Madau, P., & Dickinson, M. 2014, *ARA&A*, 52, 415, doi: [10.1146/annurev-astro-081811-125615](https://doi.org/10.1146/annurev-astro-081811-125615)
- Maiolino, R., Risaliti, G., Signorini, M., et al. 2025, *MNRAS*, 538, 1921, doi: [10.1093/mnras/staf359](https://doi.org/10.1093/mnras/staf359)
- Marconi, A., Risaliti, G., Gilli, R., et al. 2004, *MNRAS*, 351, 169, doi: [10.1111/j.1365-2966.2004.07765.x](https://doi.org/10.1111/j.1365-2966.2004.07765.x)
- Martocchia, S., Piconcelli, E., Zappacosta, L., et al. 2017, *A&A*, 608, A51, doi: [10.1051/0004-6361/201731314](https://doi.org/10.1051/0004-6361/201731314)
- Masini, A., Hickox, R. C., Carroll, C. M., et al. 2020, *ApJS*, 251, 2, doi: [10.3847/1538-4365/abb607](https://doi.org/10.3847/1538-4365/abb607)
- Merloni, A., Bongiorno, A., Bolzonella, M., et al. 2010, *ApJ*, 708, 137, doi: [10.1088/0004-637X/708/1/137](https://doi.org/10.1088/0004-637X/708/1/137)
- Miller, B. P., Gallo, E., Greene, J. E., et al. 2015, *ApJ*, 799, 98, doi: [10.1088/0004-637X/799/1/98](https://doi.org/10.1088/0004-637X/799/1/98)
- Miyaji, T., Hasinger, G., Salvato, M., et al. 2015, *ApJ*, 804, 104, doi: [10.1088/0004-637X/804/2/104](https://doi.org/10.1088/0004-637X/804/2/104)
- Nandra, K., Laird, E. S., Aird, J. A., et al. 2015, *ApJS*, 220, 10, doi: [10.1088/0067-0049/220/1/10](https://doi.org/10.1088/0067-0049/220/1/10)
- Nandra, K., Waddell, S. G. H., Liu, T., et al. 2025, *A&A*, 693, A212, doi: [10.1051/0004-6361/202449416](https://doi.org/10.1051/0004-6361/202449416)
- Narayan, R., & Yi, I. 1995, *ApJ*, 452, 710, doi: [10.1086/176343](https://doi.org/10.1086/176343)
- Ni, Q., Brandt, W. N., Chen, C.-T., et al. 2021, *ApJ*, 256, 21, doi: [10.3847/1538-4365/ac0dc6](https://doi.org/10.3847/1538-4365/ac0dc6)
- Peca, A., Cappelluti, N., Urry, C. M., et al. 2023, *ApJ*, 943, 162, doi: [10.3847/1538-4357/acac28](https://doi.org/10.3847/1538-4357/acac28)
- Peca, A., Cappelluti, N., LaMassa, S., et al. 2024, *ApJ*, 974, 156, doi: [10.3847/1538-4357/ad6df4](https://doi.org/10.3847/1538-4357/ad6df4)
- Pierre, M., Pacaud, F., Adami, C., et al. 2016, *A&A*, 592, A1, doi: [10.1051/0004-6361/201526766](https://doi.org/10.1051/0004-6361/201526766)
- Pouliasis, E., Ruiz, A., Georgantopoulos, I., et al. 2024, *A&A*, 685, A97, doi: [10.1051/0004-6361/202348479](https://doi.org/10.1051/0004-6361/202348479)
- Reines, A. E., & Volonteri, M. 2015, *ApJ*, 813, 82, doi: [10.1088/0004-637X/813/2/82](https://doi.org/10.1088/0004-637X/813/2/82)
- Reynolds, C. S., Kara, E. A., Mushotzky, R. F., et al. 2023, in *Society of Photo-Optical Instrumentation Engineers (SPIE) Conference Series*, Vol. 12678, UV, X-Ray, and Gamma-Ray Space Instrumentation for Astronomy XXIII, ed. O. H. Siegmund & K. Hoadley, 126781E, doi: [10.1117/12.2677468](https://doi.org/10.1117/12.2677468)
- Rosas-Guevara, Y. M., Bower, R. G., Schaye, J., et al. 2015, *MNRAS*, 454, 1038, doi: [10.1093/mnras/stv2056](https://doi.org/10.1093/mnras/stv2056)
- Schulze, A., Bongiorno, A., Gavignaud, I., et al. 2015, *MNRAS*, 447, 2085, doi: [10.1093/mnras/stu2549](https://doi.org/10.1093/mnras/stu2549)
- Shen, Y., & Kelly, B. C. 2012, *ApJ*, 746, 169, doi: [10.1088/0004-637X/746/2/169](https://doi.org/10.1088/0004-637X/746/2/169)

- Suh, H., Civano, F., Trakhtenbrot, B., et al. 2020, *ApJ*, 889, 32, doi: [10.3847/1538-4357/ab5f5f](https://doi.org/10.3847/1538-4357/ab5f5f)
- Suh, H., Hasinger, G., Steinhardt, C., Silverman, J. D., & Schramm, M. 2015, *ApJ*, 815, 129, doi: [10.1088/0004-637X/815/2/129](https://doi.org/10.1088/0004-637X/815/2/129)
- Takada, M., Ellis, R. S., Chiba, M., et al. 2014, *PASJ*, 66, R1, doi: [10.1093/pasj/pst019](https://doi.org/10.1093/pasj/pst019)
- Trakhtenbrot, B., & Netzer, H. 2010, *MNRAS*, 406, L35, doi: [10.1111/j.1745-3933.2010.00876.x](https://doi.org/10.1111/j.1745-3933.2010.00876.x)
- Treister, E., Schawinski, K., Urry, C. M., & Simmons, B. D. 2012, *ApJL*, 758, L39, doi: [10.1088/2041-8205/758/2/L39](https://doi.org/10.1088/2041-8205/758/2/L39)
- Ueda, Y., Akiyama, M., Hasinger, G., Miyaji, T., & Watson, M. G. 2014, *ApJ*, 786, 104, doi: [10.1088/0004-637X/786/2/104](https://doi.org/10.1088/0004-637X/786/2/104)
- Ueda, Y., Akiyama, M., Ohta, K., & Miyaji, T. 2003, *ApJ*, 598, 886, doi: [10.1086/378940](https://doi.org/10.1086/378940)
- Vasudevan, R. V., & Fabian, A. C. 2007, *MNRAS*, 381, 1235, doi: [10.1111/j.1365-2966.2007.12328.x](https://doi.org/10.1111/j.1365-2966.2007.12328.x)
- Vito, F., Brandt, W. N., Stern, D., et al. 2018, *MNRAS*, 474, 4528, doi: [10.1093/mnras/stx3120](https://doi.org/10.1093/mnras/stx3120)
- Wang, T., Liu, G., Cai, Z., et al. 2023, *Science China Physics, Mechanics, and Astronomy*, 66, 109512, doi: [10.1007/s11433-023-2197-5](https://doi.org/10.1007/s11433-023-2197-5)
- Weaver, J. R., Davidzon, I., Toft, S., et al. 2023, *A&A*, 677, A184, doi: [10.1051/0004-6361/202245581](https://doi.org/10.1051/0004-6361/202245581)
- Webb, N. A., Coriat, M., Traulsen, I., et al. 2020, *A&A*, 641, A136, doi: [10.1051/0004-6361/201937353](https://doi.org/10.1051/0004-6361/201937353)
- Whitaker, K. E., Franx, M., Leja, J., et al. 2014, *ApJ*, 795, 104, doi: [10.1088/0004-637X/795/2/104](https://doi.org/10.1088/0004-637X/795/2/104)
- Xue, Y. Q., Luo, B., Brandt, W. N., et al. 2016, *ApJS*, 224, 15, doi: [10.3847/0067-0049/224/2/15](https://doi.org/10.3847/0067-0049/224/2/15)
- Xue, Y. Q., Brandt, W. N., Luo, B., et al. 2010, *ApJ*, 720, 368, doi: [10.1088/0004-637X/720/1/368](https://doi.org/10.1088/0004-637X/720/1/368)
- Yan, W., Brandt, W. N., Zou, F., et al. 2023, *ApJ*, 951, 27, doi: [10.3847/1538-4357/accea6](https://doi.org/10.3847/1538-4357/accea6)
- Yang, G., Brandt, W. N., Alexander, D. M., et al. 2019, *MNRAS*, 485, 3721, doi: [10.1093/mnras/stz611](https://doi.org/10.1093/mnras/stz611)
- Yang, G., Estrada-Carpenter, V., Papovich, C., et al. 2021, *ApJ*, 921, 170, doi: [10.3847/1538-4357/ac2233](https://doi.org/10.3847/1538-4357/ac2233)
- Yang, G., Brandt, W. N., Vito, F., et al. 2018, *MNRAS*, 475, 1887, doi: [10.1093/mnras/stx2805](https://doi.org/10.1093/mnras/stx2805)
- Yang, G., Caputi, K. I., Papovich, C., et al. 2023, *ApJL*, 950, L5, doi: [10.3847/2041-8213/acd639](https://doi.org/10.3847/2041-8213/acd639)
- Yu, Z., Zou, F., & Brandt, W. N. 2023, *Research Notes of the American Astronomical Society*, 7, 248, doi: [10.3847/2515-5172/ad0ed7](https://doi.org/10.3847/2515-5172/ad0ed7)
- Yuan, F., & Narayan, R. 2014, *ARA&A*, 52, 529, doi: [10.1146/annurev-astro-082812-141003](https://doi.org/10.1146/annurev-astro-082812-141003)
- Zou, F., Yu, Z., Brandt, W. N., et al. 2024, *ApJ*, 964, 183, doi: [10.3847/1538-4357/ad27cc](https://doi.org/10.3847/1538-4357/ad27cc)
- Zou, F., Brandt, W. N., Chen, C.-T., et al. 2022, *ApJS*, 262, 15, doi: [10.3847/1538-4365/ac7bdf](https://doi.org/10.3847/1538-4365/ac7bdf)
- Zou, F., Gallo, E., Seth, A. C., et al. 2025, *ApJ*, 992, 176, doi: [10.3847/1538-4357/ae06a1](https://doi.org/10.3847/1538-4357/ae06a1)